Submitted to The Astrophysical Journal

The *Swift* UVOT Stars Survey. II. RR Lyrae Stars in M 3 and M 15

Michael H. Siegel[1], Blair L. Porterfield[1,2], Benjamin G. Balzer[1], Lea M. Z. Hagen[1,3]

ABSTRACT

We present the first results of an near-ultraviolet (NUV) survey of RR Lyrae stars from the Ultraviolet Optical Telescope (UVOT) aboard the *Swift Gamma-Ray Burst Mission*. It is well-established that RR Lyrae have large amplitudes in the far- and near-ultraviolet. We have used UVOT's unique wide-field NUV imaging capability to perform the first systematic NUV survey of variable stars in the Galactic globular clusters M 3 and M 15. We identify 280 variable stars, comprising 275 RR Lyrae, two anomalous Cepheids, one classical Cepheid, one SX Phoenicis star and one possible long-period or irregular variable. Only two of these are new discoveries. We compare our results to previous investigations and find excellent agreement in the periods with significantly larger amplitudes in the NUV. We map out, for the first time, an NUV Bailey diagram from globular clusters, showing the usual loci for fundamental mode RRab and first overtone RRc pulsators. We show the unique sensitivity of NUV photometry to both the temperatures and the surface gravities of RR Lyrae stars. Finally, we show evidence of an NUV period-metallicity-luminosity relationship. Future investigations will further examine the dependence of NUV pulsation parameters on metallicity and Oosterhoff classification.

Subject headings: stars: variables: RR Lyrae; globular clusters: individual (M 3, M 15); ultraviolet: stars

[1]Pennsylvania State University, Department of Astronomy, 525 Davey Laboratory, University Park, PA, 16802 (siegel@astro.psu.edu, blp14@psu.edu, bgb5080@psu.edu, lea.zernow.hagen@gmail.com)

[2]Current Address: Space Telescope Science Institute, 3700 San Martin Drive, Baltimore, MD, 21218

[3]The Institute for Gravitation and the Cosmos, The Pennsylvania State University, University Park, PA, 16801

1. Introduction

RR Lyrae stars are moderate-mass horizontal branch (HB) stars with temperatures in the range of 6000-7600 K. These "cluster variables" have been studied for over a century and become a key part of both the cosmic distance ladder and our understanding of the astrophysics of pulsating stars (see review in Smith 1995). Tens of thousands of RR Lyrae have been identified in the Milky Way, of which several thousand are in old globular clusters (Clement et al. 2001, hereafter C01).

Since the early studies of Hardie (1955) and Baker & Baker (1956), it has been known that RR Lyrae stars have exceptionally large pulsations in the ultraviolet (UV), with amplitudes of 2-8 magnitudes (Hutchinson et al. 1977; Bonnell et al. 1982; Guhathakurta et al. 1994; Downes et al. 2004; Wheatley et al. 2005, 2012; Dieball et al. 2007; Thomson et al. 2010). These exceptionally large pulsations are due to the RR Lyrae occupying a unique niche in temperature-surface gravity space, where their oscillations cause the UV flux to wax and wane dramatically. These large pulsations could allow unique insight into the underlying astrophysics. For example, the predicted UV fluxes of RR Lyrae stars at maximum and minimum light are very sensitive to the particulars of underlying atmospheric models (see, e.g., Wheatley et al. 2005), with temperature sensitivity at the 100-200 K level. UV light also probes different regions of stellar atmospheres than optical light, allowing UV light curves to provide important constraint on hydrodynamical models of stellar pulsation, including the effect of shocks on the outer stellar envelope (see, e.g., Hutchinson et al. 1977; Bonnell et al. 1982).

UV light curves could also improve the utility of RR Lyrae stars as distance indicators. Estimating distances to stellar populations using RR Lyrae stars is subject to a number of uncertainties that limit the precision of the method to about ± 0.1 mag. However, the NIR passbands bypass the issues that complicate distance measures and provide more reliable and precise RR Lyrae-based distances (see, e.g., Bono et al., 2001; Del Principe et al. 2005; Sollima et al. 2006; Neeley et al. 2015). The horizontal branch in the NIR is diagonal, producing a direct relationship between period, luminosity and metallicity. The horizontal branch is also diagonal in the NUV and FUV (Ferraro & Paresce, 1993, Dieball et al. 2007; Sandquist et al. 2010; Schiavon et al. 2012, Siegel et al. 2014, hereafter Paper I). A correlation between NUV color and magnitude indicates a correlation between stellar temperature and magnitude and, thus, a likely correlation between pulsational period and NUV magnitude similar to the one identified in the NIR. If such a relationship were proven, a metallicity and pulsation period for an RR Lyrae would yield its absolute magnitude independent of reddening. This would make RR Lyrae stars potent probes of local stellar populations and reddening, the latter of which is highly uncertain in the UV (see, e.g., Pei 1992).

The most thorough surveys in the UV are those of Downes et al. (2004), who presented partial light curves of 11 RR Lyrae in NGC 1852 using *Hubble Space Telescope* data and Wheatley et al. (2012), who presented detailed light curves for seven field RR Lyrae using GALEX data. Both studies show remarkable high-amplitude pulsations of up to eight magnitudes in the FUV. To date, however, no study has presented detailed NUV or FUV light curves of RR Lyrae stars in a globular cluster. We now fill this gap with a survey of two Galactic globular clusters – M 3 and M 15 – that have rich populations of well-studied RR Lyrae stars and represent the two poles of Oosterhoff (1939) dichotomy.

M 3 (NGC 5272) has the most well-studied population of variable stars of any Galactic globular cluster. Indeed, one of the earliest indications that RR Lyrae stars have large UV pulsations was from the study of M 3 by Baker & Baker (1956). C01 list 290 variable stars in M 3, 236 of which are RR Lyrae. These stars have been the target of decades worth of study, most recently by Kaluzny et al. (1998), Carretta et al. (1998), Bakos et al. (2000), Corwin & Carney (2001), Hartmann et al. (2005), Cacciari et al. (2005; hereafter CCC05) and Benko et al. (2006). These studies have detailed M 3's abundant family of RR Lyrae stars and shown it to be a paradigm – indeed *the* paradigm – of an Oosterhoff I (OoI) cluster, with a lower proportion of first-overtone RRc stars, shorter fundamental mode RRab periods and a shorter minimum RRab period. M 3 is often used as the baseline with which to measure the period-shift effect – the increase or decrease in the period of RR Lyrae stars in comparison to stars of equal pulsational amplitude (see Sandage 1981a, 1981b; Carney et al. 1992)

M 15 (NGC 7078) has also been studied extensively, as detailed in C01. Studies by Rosino (1950, 1969), Filippenko & Simon (1981), Sandage et al. (1981), Bingham (1984), Silberman & Smith (1995), Butler et al. (1998) Tuairisg et al. (2003), Zheleznyak & Kravtsov (2003) and Corwin et al (2008, hereafter C08) have revealed a rich population of RR Lyrae stars that are a paradigm of a metal-poor Oosterhoff II (OoII) cluster, with a high proportion of RRc stars, longer RRab periods and a longer minimum RRab period.

While both these clusters have been studied exhaustively in the optical and infrared, neither of these clusters has been thoroughly studied in the UV. In this paper, we present the first thorough NUV catalog of the variable stars of these two clusters using data from the *Swift Gammy-Ray Burst Mission*'s Ultraviolet-Optical Telescope (UVOT). Almost all of the variables studied are RR Lyrae stars, with a handful of other variable types also detected. Our analysis will therefore be focused on the RR Lyrae, investigating basic aspects of their pulsational properties and laying the groundwork for future investigations of additional clusters.

2. Observations and Data Reductions

The data presented in this analysis are entirely from the UVOT aboard the Swift mission (Gehrels et al., 2004). UVOT is a modified Richey-Chretien 30 cm telescope that has a wide (17' × 17') field of view and a microchannel plate intensified CCD operating in photon counting mode (see details in Roming et al. 2000, 2004, 2005). The instrument is equipped with a filter wheel that includes a clear white filter, u, b and v optical filters, $uvw1$, $uvm2$ and $uvw2$ ultraviolet filters, a magnifier, two grisms and a blocked filter. Although its primary mission is to measure the optical/ultraviolet afterglows of gamma ray bursts, the wide field, 2.″3 resolution, broad wavelength range (1700-8000 Å) and ability to observe simultaneously with *Swift*'s X-Ray Telescope (XRT; Burrows et al. 2005) allow a broad range of science, including the study of hot or highly energetic stars (Paper I). It is well-suited to the study of star clusters due to its field size and resolution.

Our light curves are derived from observations taken with UVOT's $uvm2$ filter, which has a central wavelength of 2246 Å and a red leak from optical light of less than 0.19% (Paper I). This was chosen to minimize potential contamination from the optical to produce as clean an NUV light curve as possible (the $uvw1$ and $uvw2$ filters have optical sensitivities of 11% and 2.4%, respectively). M 3 was observed on August 2011 as part of a Swift team fill-in program. It was then observed 11 March 2012 through 6 June 2012 approximately every 4-8 days as part of MHS's team fill-in program, then again from 4 April 2013 to 29 March 2014 as part of MHS's approved Guest Investigator program. M 15 was observed in May and August of 2011 as a Target Of Opportunity, every four days from April 2013 to March of 2014 as part of MHS's approved Guest Investigator program and then again in October of 2014 as a team fill-in. Table 1 contains a summary of the observations.

For the monitoring program, each cluster was scheduled for a nominal 1 ks for each

Table 1. Swift/UVOT Observations of Globular Clusters

Cluster	N Obs	$uvw1$ Exp Time (ks)	$uvm2$ Exp Time (ks)	$uvw2$ Exp Time (ks)	Observation Dates
M 3	67	1359	61400	1933	2011-08-31
	...	...	...	...	2012-03-11 – 2012-06-12
	...	...	...	...	2013-04-04 – 2014-03-29
M 15	55	5203	44849	287	2011-05-18 – 2011-08-28
	...	...	...	...	2013-04-11 – 2014-03-31
	...	...	...	...	2014-10-16

observation. However, Swift's planning sometimes broke that observation up over two or more orbits, separated by some multiple of Swift's 96-minute orbital period. Observations that were not performed as part of the monitoring campaign were sometimes performed in modes that did not include $uvm2$. Additionally, some observations were curtailed or cancelled by gamma-ray bursts or high-priority targets or had trailed images. In the end, our analysis of M 3 is based on 85 individual $uvm2$ images and M 15 from 48 individual $uvm2$ images.

Photometry was derived using DAOPHOT/ALLFRAME (Stetson 1987, 1994). The details of this process can be found in Paper I. To briefly summarize: we created individual images for each observation from the archival data downloaded from HEASARC, regenerating the exposure maps and large-scale sensitivity images for calibration. After running DAOPHOT on the individual fields, the images were then put through ALLFRAME to derive consistent deep photometry on all fields. We then calibrated the instrumental photometry to the standard system (Poole et al. 2008; Breeveld at al. 2010, 2011) correcting for coincidence loss, variation in exposure time and large-scale sensitivity.

Figures 1 and 2 show the color-magnitude diagrams of M 3 and M 15, respectively. We should $uvm2 - uvw1$ on the left and $uvw2 - uvw1$ on the right. In both cases, we have only plotted stars with DAOPHOT SHARP parameters of 0.5 or less. SHARP is a structural parameter produced by DAOPHOT that measures the difference between the isophotal and peak magnitudes. We have found it to be the most effective means of identifying poor measures in UVOT data and, in these cases, it mostly excludes stars from the burned-in cores of the clusters.

The most visible features are the diagonal horizontal branches, with the RR Lyrae gap visible in the increased scatter around the HB locus. The faint haze of stars at the bottom of the CMD are mostly bright RGB and field stars detected by the red leak.

2.1. Light Curve Fitting

Variable stars were selected for light curve fitting using the variability index measured by the DAOMASTER code included with DAOPHOT. Any star with a photometric scatter more than three times the formal error was selected as a potential variable star. We further refined the list by only selecting stars with DAOPHOT SHARP values less than 0.5. This excluded many stars that were within the burned-in core of the cluster.

Our first pass at the light curves used the RRFIT code of Yang & Sarajedini (2012), which fits the light curves using the light curve templates of Layden (1998) as well as those

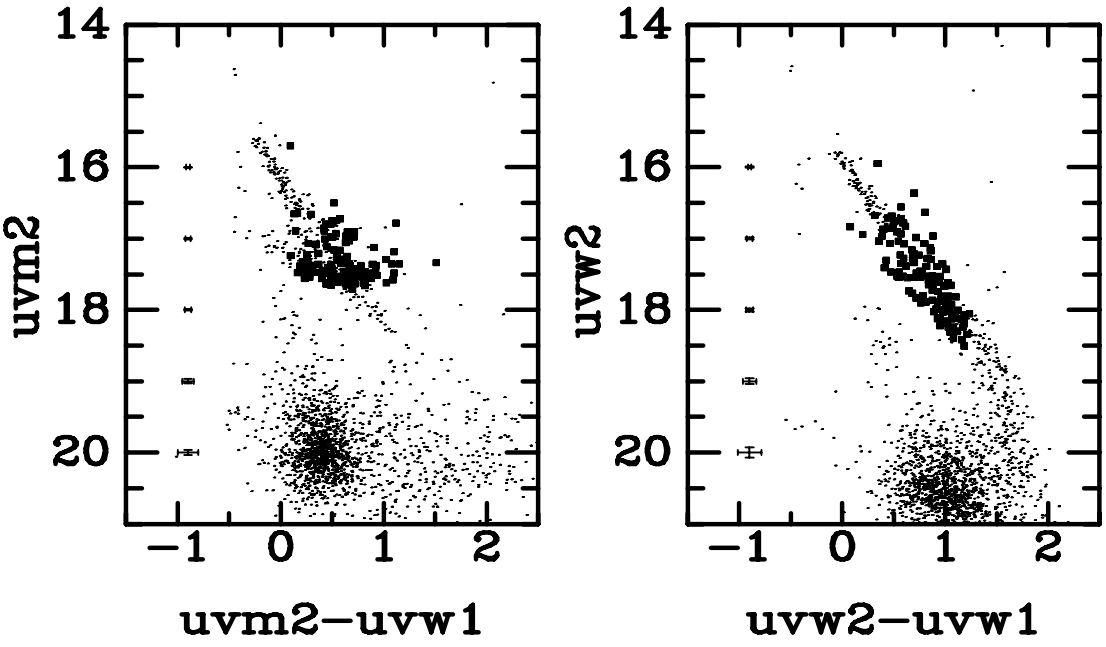

Fig. 1.— UVOT color-magnitude diagrams of the globular cluster M 3. The left panel plots $uvm2$ against $uvw1$ while the right plot $uvw2$ against $uvw1$. The prominent diagonal sequence is the HB. Blue stragglers, AGB manque stars and other hot star types are present, as detailed in Paper I. The squares mark RR Lyrae identified in this study. Error bars on the left side indicate typical uncertainties.

of Kovacs & Kupi (2007). These templates are drawn from a sample of RR Lyrae stars and represent a wide variety of light curve shapes. The drawback of template-fitting is that it can be confused by second order variations such as the Blazhko (1907) effect or double-mode pulsation. It also may not be entirely appropriate to NUV data, which may have different light curve shapes than the optical data on which the templates are based. Finally, our search parameters only covered periods between 0.2 to 1.2 days, which would exclude most SX Phoenicis stars, Cepheids and long-period variables. Nevertheless, this provided a good first estimate of the periods and amplitudes for the vast majority of the variable stars in these two systems.

After preliminary fits were obtained with RRFIT, we ran each of our stars through

IRAF's phase-dispersion minimization algorithm to both refine the period and provide an eyeball check on the fits. For almost all stars, the two methods agreed. For those where there was some disagreement due to multiple minima in the periodogram, we used the period with the lowest phase dispersion. For a handful of stars, neither method produced a satisfactory result.

After fitting the light curves based on UVOT data, we compared our results to the comprehensive C01 catalog of globular cluster variable stars. We pulled out for analysis any variable star candidates from C01 that had not been selected as variable star candidates from the UVOT data (either because their variability index was too low or their SHARP parameter too high) For most of these, we were able to fit periods and amplitudes using the UVOT data, both with template-fitting and with phase dispersion minimization.

Tables 2 and 3 provide the catalog of variable stars, with identification numbers taken from C01. Where we have identified new variable stars, we have added new identification numbers sequential to C01. The columns list C01 identification number, equatorial coordinates, periods, amplitudes and mean magnitudes derived from the $UVOT$ data. The last two columns list the variability index and the SHARP parameter as calculated by DAOPHOT. Tables 4 and 5 give the Julian Dates, $uvm2$ measures and measurement uncertainties for the variable stars.

Figure 3 shows the light curves for all of the RR Lyrae stars in M 3, ordered by increasing period. Figure 11 shows the light curves of the other variable stars measured in M 3 and Figure 12 shows the light curve of a possible long-period or irregular variable. Figures 13 shows the light curves for all of the RR Lyrae stars in M 15, ordered by increasing period. Figure 17 shows the light curves of the other variable stars measured in M 15.

One of the pitfalls of using previous catalogs to pull marginal detections out of the noise is that the light curves of such stars are less than ideal. UVOT's comparatively coarse resolution means that stars in the cores of globular clusters frequently have their light blended with that of nearby stars. This tends to increase the magnitudes and dampen the amplitudes of any pulsations, muddying the correlations between pulsation parameters (see §3). This can be seen visually in Figures 3 through 17, where we have marked with asterisks stars with DAOPHOT SHARP values greater than 0.5 – which indicates a broad PSF. These stars are found almost exclusively in the burned-in cores of the clusters.

The effect of blends on the UVOT photometry is complicated, raising the measured count rate but also increasing the coincidence loss. It is impossible to remove their contribution without making *a priori* assumptions about the variable stars or their unresolved companions. We include these stars in the compilation but caution that their $uvm2$ mag-

nitudes and A_{uvm2} amplitudes are **not reliable** and should be excluded from any global analysis of the variable stars.

For completeness, our tables include mean magnitudes, variability and SHARP values for stars which we have matched to the C01 catalog but are unable to fit a period. This includes stars that C01 classify as non-variable. However, these stars are only included if the SHARP value is less than 0.5. Stars with SHARP values greater than 0.5 may be blends and are much more likely to be have been misidentified or have their pulsations drowned in the light of nearby star.

Table 2. Parameters of Variable Stars in M 3

ID (C01)	α (J2000.0)	δ	P (days)	$< uvm2 >_i$	A_{uvm2}	Var	SHARP
V1	13:42:11.11	28:20:33.5	0.5205563	17.338	2.382	6.60	0.15
V3	13:42:15.70	28:21:41.0	0.5581785	17.289	2.438	4.19	0.35
V4*	13:42:08.19	28:22:32.9	0.5850817	16.395	1.125	5.22	0.66
V5	13:42:31.26	28:22:20.4	0.5058278	17.116	1.650	6.43	0.28
V6	13:42:02.06	28:23:41.3	0.5143057	17.516	2.320	4.66	0.27
V7	13:42:11.08	28:24:09.9	0.4974221	17.305	2.341	5.74	0.49
V8	13:42:05.32	28:22:18.4	0.6367176	16.784	0.709	5.20	0.29
V9	13:41:49.50	28:19:13.3	0.5415324	17.463	2.316	4.54	0.14
V10	13:42:23.08	28:25:00.2	0.5695330	17.459	1.764	5.32	0.19
V11	13:41:59.97	28:19:11.7	0.5078967	17.239	2.181	5.81	0.35
V12	13:42:11.25	28:20:16.8	0.3179041	16.750	0.898	6.33	0.41
V13	13:42:09.57	28:20:24.3	0.4795181	17.163	1.183	6.62	0.19
V14	13:42:07.79	28:20:00.9	0.6358649	17.546	2.131	6.98	0.12
V15	13:42:04.66	28:18:08.5	0.5300817	17.385	2.268	5.92	0.21
V16	13:41:48.70	28:21:07.9	0.5114729	17.507	2.312	4.31	0.26
V17	13:42:22.40	28:15:22.6	0.5761198	17.528	1.401	6.32	0.14
V18	13:42:18.94	28:17:47.0	0.5164755	17.597	2.341	5.34	0.10
V19	13:42:38.10	28:18:37.5	0.6320068	17.709	1.207	4.18	0.14
V20	13:42:36.81	28:18:11.5	0.4912951	17.185	1.924	6.42	0.17
V21	13:42:37.76	28:23:01.3	0.5157982	17.558	2.406	5.01	0.15
V22	13:42:25.89	28:22:31.6	0.4813960	17.298	2.212	6.05	0.12
V23	13:42:02.83	28:27:20.1	0.5954373	17.465	1.462	5.16	0.21
V24	13:42:00.30	28:22:51.6	0.6634306	17.460	1.799	5.01	0.26
V25	13:42:02.07	28:22:09.9	0.4800817	17.372	2.316	3.71	0.13
V26	13:41:58.03	28:21:58.2	0.5977560	17.328	1.948	5.31	0.28
V27	13:42:03.16	28:20:58.8	0.5790610	17.579	1.801	5.46	-0.20
V28	13:42:09.61	28:20:56.2	0.4706749	17.122	1.338	6.63	0.18
V29*	13:42:06.64	28:21:27.4	0.4717771	16.318	0.690	5.03	0.84
V30	13:42:08.73	28:23:39.6	0.5120514	17.373	2.284	5.97	0.15
V31	13:42:13.99	28:23:47.2	0.5807016	17.661	2.363	5.88	-0.25
V32*	13:42:12.38	28:23:41.9	0.4953458	17.054	1.821	4.92	0.51
V33	13:42:16.82	28:21:13.0	0.5252704	17.349	1.808	5.30	-0.15
V34	13:42:21.70	28:25:32.2	0.5591055	17.445	1.471	7.37	0.10
V35	13:42:03.43	28:18:03.4	0.5305683	17.362	1.713	6.21	0.21
V36	13:42:24.52	28:22:07.1	0.5455711	17.509	2.158	5.20	0.09
V37	13:41:53.55	28:25:25.2	0.3266509	16.931	1.015	7.29	0.19

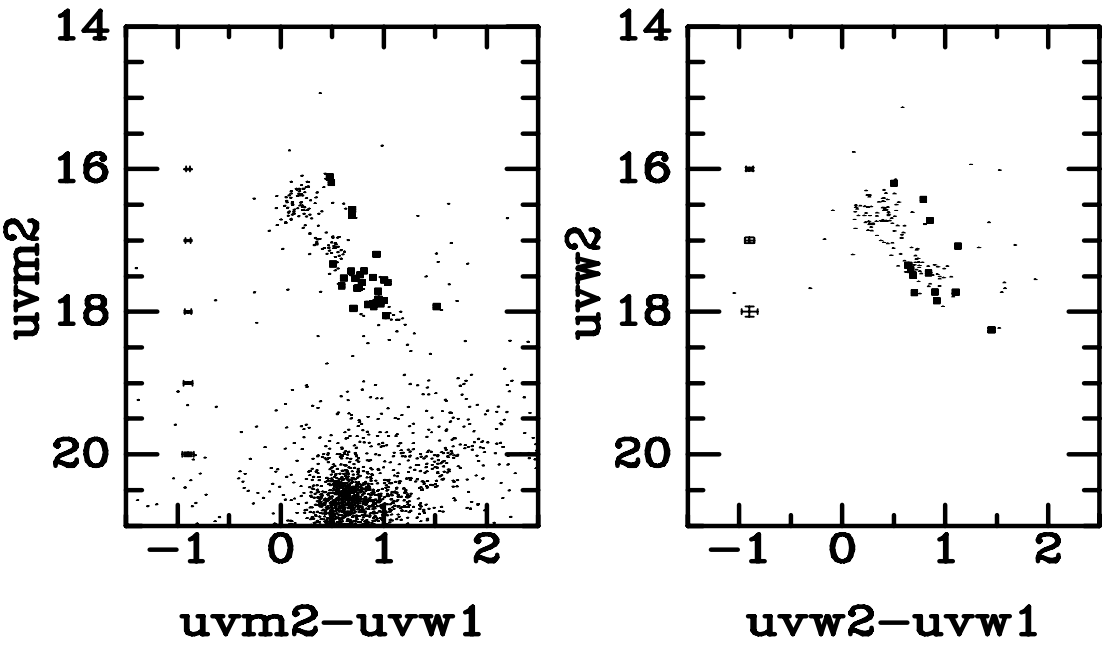

Fig. 2.— UVOT color-magnitude diagrams of the globular cluster M 15. The left panel plots $uvm2$ against $uvw1$ while the right plot $uvw2$ against $uvw1$. The prominent diagonal sequence is the HB. Blue stragglers, AGB manque stars and other hot star types are present, as detailed in Paper I. The $uvw2$ data are very shallow due to the very small amount of time invested in the filter during the observational campaign. The squares mark RR Lyrae identified in this study. Error bars on the left side indicate typical uncertainties.

Table 2—Continued

ID (C01)	α (J2000.0)	δ	P (days)	$< uvm2 >_i$	A_{uvm2}	Var	SHARP
V38	13:41:56.04	28:24:48.6	0.5580155	17.480	1.604	6.91	0.10
V39	13:41:52.96	28:24:42.0	0.5870736	17.597	1.472	6.17	0.04
V40	13:41:50.93	28:24:32.6	0.5515324	17.611	2.100	4.57	0.13
V41	13:42:04.37	28:23:35.5	0.4850817	17.447	2.418	5.23	-0.20
V42	13:42:05.50	28:23:22.0	0.5900818	17.225	2.062	5.90	0.26
V43	13:42:19.05	28:23:06.6	0.5404946	17.545	2.084	5.40	-0.18
V44	13:42:24.35	28:24:21.7	0.5065204	17.219	1.450	7.00	0.16
V45	13:41:53.22	28:20:31.1	0.5368882	17.548	1.992	6.40	0.10
V46	13:42:01.80	28:21:50.2	0.6133907	17.559	1.218	4.67	0.43
V47	13:42:02.59	28:21:28.5	0.5410013	17.356	1.666	6.87	0.16
V48	13:42:21.15	28:21:00.1	0.6279041	17.380	1.340	5.08	0.33
V49	13:42:22.09	28:21:02.4	0.5482007	17.463	1.716	7.85	0.34
V50	13:42:12.22	28:18:47.8	0.5131192	17.373	1.971	6.66	0.05
V51	13:42:13.85	28:18:55.8	0.5840006	17.583	1.688	4.65	0.11
V52*	13:42:05.62	28:25:12.8	0.5162355	17.212	1.633	5.57	0.90
V53	13:42:10.92	28:24:44.5	0.5048887	17.356	2.084	4.67	0.17
V54	13:42:08.98	28:24:28.2	0.5061939	17.209	1.366	5.93	0.11
V55	13:41:55.91	28:28:05.3	0.5298442	17.517	2.188	4.36	0.10
V56	13:42:00.67	28:28:39.4	0.3296071	16.892	0.926	6.74	0.12
V57	13:42:23.23	28:22:41.9	0.5121922	17.493	2.354	3.95	-0.01
V58*	13:42:04.94	28:23:27.6	0.5170514	17.169	2.125	5.60	0.56
V59	13:42:03.23	28:18:53.1	0.5887867	17.636	1.779	5.81	0.17
V60	13:41:49.05	28:17:25.5	0.7077409	17.592	1.729	5.08	0.21
V61	13:42:25.77	28:28:45.3	0.5209119	17.366	1.649	7.87	0.14
V62	13:42:18.21	28:29:38.7	0.6524221	17.639	1.440	5.11	0.26
V63	13:42:14.22	28:28:23.6	0.5703336	17.557	1.962	6.17	0.17
V64	13:42:20.10	28:28:12.0	0.6054125	17.623	1.476	5.00	0.27
V65	13:42:20.90	28:28:09.6	0.6683648	17.473	1.994	14.60	0.26
V66	13:42:03.76	28:24:42.4	0.6201262	17.553	1.256	6.18	0.35
V67	13:42:01.50	28:24:44.0	0.5683120	17.499	1.720	4.24	0.46
V68	13:42:13.08	28:25:36.7	0.3559851	16.977	1.104	7.49	0.34
V69	13:42:17.56	28:25:03.0	0.5666287	17.607	1.999	5.51	0.09
V70	13:42:14.32	28:25:14.0	0.4861218	16.979	0.694	6.66	0.11
V71	13:42:23.63	28:22:40.0	0.5490881	17.505	1.718	6.24	0.13
V72	13:42:45.23	28:22:40.9	0.4561051	17.360	2.436	3.82	0.19
V73	13:42:44.70	28:23:45.4	0.6734648	17.624	0.647	4.73	0.29

Table 2—Continued

ID (C01)	α (J2000.0)	δ	P (days)	$< uvm2 >_i$	A_{uvm2}	Var	SHARP
V74	13:42:18.13	28:25:12.7	0.4921432	17.427	2.333	5.41	0.24
V75	13:42:15.12	28:25:21.0	0.3140880	16.903	0.928	7.56	0.21
V76	13:42:10.40	28:21:13.8	0.5017919	17.539	2.549	5.44	-0.16
V77	13:42:04.28	28:23:09.3	0.4593696	17.472	2.717	5.10	-0.02
V78	13:42:15.05	28:23:48.3	0.6118882	17.406	1.340	5.43	-0.00
V79	13:42:14.70	28:28:31.2	0.4833121	17.373	2.432	5.75	0.23
V80	13:42:43.02	28:27:27.5	0.5384485	17.434	2.130	6.30	0.01
V81	13:42:37.35	28:28:33.9	0.5291203	17.464	2.254	4.06	0.18
V83	13:41:38.00	28:24:33.2	0.5012950	17.477	2.403	5.56	0.10
V84	13:42:16.30	28:25:26.8	0.5957091	17.560	1.587	6.76	0.24
V85	13:42:34.64	28:26:28.7	0.3558278	16.797	1.083	10.78	0.18
V86	13:42:50.39	28:20:48.7	0.2926594	16.909	1.079	5.49	0.21
V87	13:42:19.83	28:23:42.2	0.3574923	16.852	0.711	5.35	0.37
V88	13:42:08.82	28:21:32.0	0.2987496	16.964	1.239	6.60	0.09
V89	13:42:13.61	28:20:51.3	0.5484975	17.650	2.447	6.82	-0.16
V90	13:42:18.90	28:19:33.9	0.5170495	17.465	2.257	4.78	0.29
V91*	13:42:10.56	28:13:32.2	0.5301558	17.387	2.543	25.96	0.60
V92	13:42:09.37	28:15:53.4	0.5035271	17.392	2.131	6.17	0.12
V93	13:41:47.40	28:16:04.2	0.6023110	17.581	1.598	4.58	0.18
V94	13:41:34.55	28:18:55.2	0.5237049	17.552	1.940	3.54	0.15
V96	13:41:59.11	28:18:47.3	0.4993844	17.248	2.243	4.99	0.37
V97	13:42:01.69	28:19:24.6	0.3349331	17.080	0.960	6.82	0.12
V98	13:42:21.50	28:22:38.8	···	16.418	···	1.62	0.27
V99	13:42:26.73	28:21:47.6	0.4822200	17.008	0.509	7.09	0.19
V100	13:42:16.74	28:24:19.5	0.6187912	17.620	1.366	5.46	0.16
V101	13:42:14.98	28:24:05.3	0.6439074	17.635	1.266	5.07	0.36
V102	13:42:15.86	28:24:36.9	···	17.896	···	2.00	0.32
V104	13:42:09.49	28:25:07.0	0.5699183	17.379	2.359	5.87	0.26
V105	13:42:09.84	28:25:52.9	0.2877559	16.646	0.580	5.17	0.19
V106	13:42:07.79	28:25:29.6	0.5468882	17.558	1.846	5.80	0.48
V107	13:42:05.63	28:28:16.3	0.3090314	16.927	1.105	6.03	0.18
V108	13:41:54.78	28:27:51.6	0.5196071	17.533	2.294	5.46	0.15
V109	13:42:04.71	28:22:44.0	0.5338904	17.485	2.229	5.19	0.38
V110	13:42:03.93	28:22:25.8	0.5354818	17.460	1.944	6.10	0.01
V111*	13:42:04.44	28:23:03.5	0.5102003	17.249	1.585	4.78	0.77
V117	13:42:18.38	28:14:53.9	0.6005268	17.503	1.720	5.13	0.13

Table 2—Continued

ID (C01)	α (J2000.0)	δ	P (days)	$< uvm2 >_i$	A_{uvm2}	Var	SHARP
V118	13:42:22.49	28:17:50.3	0.4993696	17.473	2.100	5.81	0.19
V119	13:42:30.65	28:24:28.5	0.5176224	17.319	2.055	4.84	0.30
V120	13:41:48.98	28:26:31.7	0.6401262	17.572	1.048	4.49	0.40
V121	13:42:08.16	28:23:37.5	0.5352151	17.482	2.035	5.87	0.02
V124	13:42:06.50	28:19:20.5	0.7524591	17.614	0.789	5.19	0.24
V125	13:42:25.62	28:20:29.9	0.3498442	17.031	0.783	5.68	0.19
V126	13:42:10.34	28:20:15.5	0.3484204	17.071	0.825	7.53	0.09
V128	13:42:20.11	28:24:53.2	0.2920440	16.797	1.060	8.24	0.22
V129	13:42:08.20	28:23:59.1	0.4060800	16.976	0.841	5.07	0.14
V130	13:42:11.76	28:24:05.9	0.5689839	17.054	0.927	4.82	0.38
V131	13:42:05.88	28:23:08.7	0.2976816	16.906	0.912	4.86	0.09
V132	13:42:07.42	28:22:19.8	0.3398590	16.892	0.751	4.76	0.38
V133	13:42:07.00	28:23:25.3	0.5507461	17.443	2.064	4.39	0.25
V134	13:42:09.77	28:23:34.2	0.6180969	17.489	1.362	4.79	0.30
V135*	13:42:09.44	28:23:20.0	0.5683759	17.292	1.392	3.95	0.65
V137*	13:42:15.45	28:22:22.9	0.5751706	17.172	1.511	3.79	0.64
V138	13:41:51.52	28:23:22.3	···	20.915	···	1.10	-0.03
V139*	13:42:14.07	28:23:10.3	0.5599315	16.917	1.798	3.51	1.30
V140	13:42:10.28	28:24:30.4	0.3331340	16.744	0.855	6.71	0.05
V142*	13:42:09.24	28:21:43.6	0.5686457	17.732	2.222	5.47	0.51
V144	13:42:15.58	28:21:02.5	0.5968290	17.420	0.829	5.03	0.32
V145*	13:42:13.72	28:22:51.1	0.5144810	15.423	0.373	1.35	1.07
V146	13:42:18.48	28:21:43.6	0.5021922	17.353	2.313	5.10	0.48
V147*	13:42:09.83	28:23:29.1	0.3464951	16.814	0.628	4.24	0.71
V149	13:42:14.07	28:23:34.8	0.5482007	17.499	2.116	4.75	0.41
V150	13:42:16.67	28:23:20.0	0.5239690	17.446	2.009	4.64	0.30
V151*	13:42:12.01	28:22:01.3	0.5168290	16.809	1.150	3.54	0.90
V152	13:42:17.45	28:23:33.2	0.3261199	16.652	0.763	6.83	0.41
V154*	13:42:11.65	28:22:14.2	15.2841997	15.418	1.151	5.13	1.04
V156*	13:42:09.95	28:22:01.3	0.5319919	17.158	1.761	4.56	0.51
V157*	13:42:10.20	28:23:19.0	0.5428745	16.101	0.458	2.08	0.90
V160*	13:42:10.79	28:21:58.8	0.6573062	17.109	1.413	4.94	0.59
V161*	13:42:12.76	28:21:44.7	0.5265768	17.017	1.340	4.57	0.64
V162*	13:42:13.57	28:22:11.1	0.5448409	15.915	0.325	1.79	0.92
V165	13:42:17.03	28:23:02.6	0.4836457	17.271	2.462	4.89	0.41
V166	13:42:04.15	28:22:34.2	0.4850076	17.159	1.038	6.69	0.19

Table 2—Continued

ID (C01)	α (J2000.0)	δ	P (days)	$< uvm2 >_i$	A_{uvm2}	Var	SHARP
V167	13:42:05.58	28:22:05.4	0.6440240	17.545	0.960	4.09	0.04
V168*	13:42:08.06	28:22:49.4	0.2759464	16.502	0.541	4.05	0.67
V170*	13:42:09.35	28:23:14.9	0.4326001	16.453	0.686	3.19	1.04
V171*	13:42:09.51	28:22:58.7	0.3032750	16.572	0.803	3.02	1.00
V172	13:42:09.86	28:23:08.3	0.5422813	17.455	1.986	4.61	0.14
V174*	13:42:10.82	28:22:09.0	0.5913617	17.098	0.955	2.90	1.42
V175*	13:42:14.65	28:23:09.0	0.5696960	17.112	1.238	2.74	1.03
V176*	13:42:14.96	28:23:15.3	0.5396516	17.263	1.639	4.92	0.72
V177	13:42:16.24	28:22:13.5	0.3483463	16.723	0.878	6.74	0.27
V178*	13:42:17.45	28:23:29.1	0.2669697	16.663	0.601	4.93	0.63
V180*	13:42:10.16	28:22:13.9	0.6091277	16.959	0.580	1.86	1.55
V182	13:42:10.10	28:23:41.5	···	18.020	···	2.13	0.37
V184*	13:42:09.58	28:22:27.7	0.5311763	17.086	1.624	2.72	1.61
V186*	13:42:12.47	28:21:39.4	0.6631933	17.327	0.911	4.55	0.80
V190*	13:42:10.89	28:23:10.7	0.5228004	17.019	1.340	3.11	1.10
V191*	13:42:11.57	28:23:05.9	0.5191869	16.262	0.697	2.53	0.56
V192*	13:42:11.32	28:22:46.9	0.4973590	15.375	0.410	2.32	1.14
V195*	13:42:10.47	28:22:14.2	0.6439052	16.937	0.521	2.68	1.35
V197	13:42:15.88	28:22:51.4	0.4999183	17.476	2.667	6.61	-0.21
V200*	13:42:11.16	28:23:03.8	0.3609884	16.717	0.761	3.59	0.79
V201*	13:42:11.81	28:22:33.8	0.5405832	15.611	0.338	1.94	0.95
V202	13:41:42.83	28:24:17.2	0.7735864	17.579	0.455	4.01	0.19
V203	13:42:09.43	28:17:30.2	0.2897997	16.661	0.277	2.98	0.22
V204	13:42:38.69	28:22:47.3	···	17.527	···	1.52	0.21
V207	13:42:14.16	28:22:11.4	0.3453130	16.500	0.478	3.11	0.41
V208*	13:42:11.59	28:21:44.3	0.3696448	15.606	0.212	2.03	0.72
V209	13:42:06.37	28:21:02.9	0.3483121	15.699	0.285	2.69	0.31
V210*	13:42:04.89	28:22:31.2	0.3529560	15.945	0.264	2.18	0.52
V211*	13:42:07.42	28:22:50.7	0.5581773	16.235	0.362	1.59	0.84
V212*	13:42:09.86	28:22:04.6	0.5421922	17.194	1.087	3.25	0.99
V213*	13:42:09.57	28:22:12.3	0.3000373	16.458	0.726	2.91	0.99
V215*	13:42:10.45	28:22:41.0	0.5287049	16.491	1.257	2.61	1.65
V216*	13:42:13.58	28:22:32.1	0.3464803	16.375	0.479	2.40	1.66
V217*	13:42:11.37	28:22:14.9	0.5283713	15.771	0.453	2.74	0.74
V219*	13:42:07.04	28:22:57.4	0.6136531	17.346	1.208	5.50	0.52
V220*	13:42:13.99	28:22:26.2	0.6001558	17.093	1.043	3.35	0.70

Table 2—Continued

ID (C01)	α (J2000.0)	δ	P (days)	$< uvm2 >_i$	A_{uvm2}	Var	SHARP
V222	13:42:18.75	28:21:38.6	0.5967771	17.292	1.513	4.13	0.39
V223*	13:42:13.24	28:22:36.2	0.3292243	16.381	0.651	2.69	1.42
V229*	13:42:08.98	28:21:55.7	0.4976213	16.471	1.288	2.98	0.57
V230	13:42:30.92	28:14:29.1	20.2900009	0.000	1.850	0.22	0.00
V231	13:42:20.91	28:23:29.2	···	16.043	···	1.22	0.17
V232	13:42:20.49	28:23:23.7	···	16.174	···	1.67	0.25
V234*	13:42:13.06	28:22:00.9	0.5080599	16.144	0.698	1.72	0.94
V235*	13:42:13.74	28:23:19.1	0.7598442	17.378	1.026	4.19	0.51
V237	13:42:15.71	28:18:16.6	···	18.590	···	2.01	0.17
V239*	13:42:09.87	28:22:14.4	0.5039691	15.671	0.504	3.14	0.57
V241*	13:42:10.76	28:22:37.4	0.5961837	16.044	0.892	2.87	1.53
V242*	13:42:13.15	28:22:24.3	0.5965099	16.027	0.474	2.41	1.21
V243*	13:42:12.32	28:22:14.3	0.6346002	15.735	0.247	2.16	0.74
V245*	13:42:09.83	28:22:58.5	0.2840314	16.231	0.520	1.87	1.61
V247*	13:42:14.74	28:22:15.4	0.6053416	17.277	0.951	2.28	1.10
V248*	13:42:09.64	28:22:48.9	0.5097782	16.501	0.780	2.86	1.26
V249*	13:42:10.41	28:22:47.4	0.6149183	16.006	0.534	1.95	1.34
V254*	13:42:12.40	28:22:53.3	0.6056276	16.192	0.523	2.12	1.02
V255*	13:42:12.65	28:22:43.8	0.5726668	15.709	0.428	2.13	1.33
V256*	13:42:13.02	28:22:57.9	0.3180525	15.891	0.312	2.21	0.93
V257*	13:42:13.03	28:22:29.0	0.6020543	15.858	0.328	1.45	1.03
V258*	13:42:14.29	28:23:30.8	0.7134203	17.522	1.311	5.22	0.58
V259*	13:42:14.55	28:22:54.3	0.3335394	16.720	0.673	4.15	0.60
V261*	13:42:10.10	28:22:39.9	0.4447997	16.122	0.396	2.77	0.81
V264*	13:42:10.86	28:22:29.9	0.3564728	15.969	0.359	2.10	1.28
V269*	13:42:12.76	28:22:31.8	0.3557017	15.278	0.200	1.60	1.30
V270*	13:42:11.94	28:23:31.1	0.6902007	15.672	0.580	4.09	0.68
V271*	13:42:12.16	28:23:18.6	0.6327827	15.516	0.200	1.85	0.70
V287	13:41:41.00	28:20:55.5	···	20.691	···	1.57	-0.03
V288	13:42:17.38	28:13:34.7	···	18.266	···	1.65	0.11
V289	13:42:12.16	28:19:20.9	···	18.201	···	1.54	0.18
V290	13:42:21.28	28:23:44.6	···	16.735	···	1.71	0.13
V291	13:42:18.05	28:22:38.4	0.0716300	18.052	0.828	2.95	0.05
V292*	13:42:11.17	28:21:53.4	0.2965601	16.567	0.387	2.93	0.57
V293	13:42:20.57	28:28:32.0	···	18.450	···	1.55	0.05
V294	13:42:13.67	28:25:30.0	···	18.520	···	1.60	0.30

Table 2—Continued

ID (C01)	α (J2000.0)	δ	P (days)	$< uvm2 >_i$	A_{uvm2}	Var	SHARP
V295	13:41:58.54	28:27:58.7	···	18.793	···	1.50	0.12
V296	13:41:42.98	28:24:03.3	···	19.714	···	2.48	0.14
V300	13:42:08.21	28:21:38.9	252.8500061	17.322	0.416	4.17	0.23

Table 3. Parameters of Variable Stars in M 15

ID (C01)	α (J2000.0)	δ	P (days)	$< uvm2 >_i$	A_{uvm2}	Var	SHARP
V1	21:29:50.16	12:10:26.1	1.4377750	17.237	1.627	8.45	0.33
V2	21:29:46.51	12:10:07.2	0.6841473	17.888	1.238	4.12	0.32
V3	21:29:41.35	12:09:13.9	0.3887274	17.512	0.960	6.83	0.16
V4	21:29:50.62	12:07:17.6	0.3135568	17.310	0.884	9.23	0.40
V5	21:29:51.50	12:06:29.0	0.3842009	17.428	0.953	5.53	0.17
V6	21:29:59.88	12:11:18.9	0.6659238	18.014	1.741	3.48	-0.21
V7	21:29:58.91	12:11:15.7	0.3675779	17.662	1.009	4.06	0.04
V8	21:29:58.15	12:12:09.4	0.6464081	17.928	1.814	3.97	0.36
V9	21:29:59.19	12:12:21.1	0.7156435	17.712	1.454	5.11	0.39
V10	21:30:06.79	12:10:04.8	0.3863821	17.670	0.910	4.97	0.24
V11	21:30:09.95	12:09:42.1	0.3432007	17.526	1.034	5.24	0.26
V12	21:30:09.32	12:09:12.7	0.5928004	17.889	1.381	5.08	0.42
V13	21:30:06.89	12:08:54.6	0.5748671	17.885	1.774	3.60	0.18
V14	21:30:04.10	12:05:47.1	0.3819919	17.637	1.093	4.86	0.06
V15	21:30:03.93	12:04:59.2	0.5835864	17.849	1.786	5.81	0.09
V16	21:30:05.03	12:12:12.5	0.3992092	17.589	0.875	6.41	0.25
V17	21:30:03.88	12:11:52.9	0.4288904	17.566	0.827	5.79	0.30
V18	21:30:03.46	12:11:43.4	0.3677503	17.501	0.986	5.30	0.15
V19	21:30:05.75	12:12:43.4	0.5723480	17.789	2.454	5.63	0.07
V20	21:30:03.73	12:09:53.0	0.6968760	18.055	1.709	3.08	0.36
V21*	21:30:00.57	12:09:05.1	0.6489394	17.674	1.404	4.68	0.55
V22	21:29:35.74	12:09:14.0	0.7202495	17.805	1.658	4.87	0.09
V23	21:30:11.17	12:14:19.6	0.6326446	17.821	1.418	5.13	0.40
V24	21:29:50.97	12:09:55.5	0.3697256	17.596	0.971	6.15	0.20
V25	21:30:18.84	12:09:53.8	0.6653631	18.021	1.484	3.52	0.30
V26	21:29:59.66	12:15:33.9	0.4023091	17.742	0.731	5.90	0.09
V27	21:30:13.28	12:14:12.3	···	20.170	···	1.33	0.30
V29	21:30:09.21	12:13:34.6	0.5747560	18.091	1.419	5.22	0.14
V30*	21:29:47.02	12:09:58.6	0.4060355	16.471	0.222	1.85	0.51
V31	21:29:50.46	12:14:06.5	0.4081596	17.670	0.808	5.26	0.18
V32	21:29:54.74	12:11:49.5	0.6053026	17.554	1.086	5.36	0.21
V33*	21:29:55.47	12:09:33.7	0.5839413	17.300	1.339	3.97	0.61
V34	21:29:54.47	12:09:07.2	2.0373480	17.651	0.688	4.65	0.28
V35	21:29:55.99	12:07:18.7	0.3839766	17.710	0.997	6.60	0.03
V36	21:29:56.36	12:08:40.8	0.6241769	17.897	1.695	4.01	0.46
V37	21:29:56.53	12:08:45.1	0.2874888	17.193	0.745	5.20	0.42

Table 3—Continued

ID (C01)	α (J2000.0)	δ	P (days)	$< uvm2 >_i$	A_{uvm2}	Var	SHARP
V38	21:29:58.80	12:07:36.3	0.3752608	17.532	1.033	4.79	0.27
V39*	21:29:59.66	12:07:58.0	0.3895853	17.553	0.628	4.20	0.61
V40	21:30:07.22	12:08:06.4	0.3773258	17.589	1.058	5.25	0.11
V41	21:30:02.55	12:09:07.6	0.3917472	17.427	0.735	4.34	0.44
V42	21:30:13.71	12:09:27.1	0.3601973	17.637	1.003	6.42	0.15
V43	21:30:26.57	12:11:48.0	0.3959861	17.649	0.923	4.69	0.19
V44	21:30:04.43	12:10:06.7	0.5959346	17.842	1.463	5.15	0.21
V45*	21:30:02.76	12:09:31.4	0.6775171	17.692	0.557	3.70	0.75
V47*	21:30:01.24	12:09:59.1	0.6874813	16.089	0.454	2.73	0.73
V48	21:30:02.22	12:12:32.8	0.3649691	17.517	1.117	5.76	0.26
V49	21:30:00.89	12:12:49.1	0.6552283	16.647	0.584	3.30	0.27
V50	21:30:09.37	12:11:43.2	0.2980822	17.467	1.017	7.26	0.22
V52	21:30:11.34	12:09:41.7	0.5756440	18.097	1.400	4.20	0.28
V53	21:29:51.99	12:08:11.3	0.4141384	17.528	0.827	4.85	0.18
V54*	21:29:58.93	12:11:30.3	0.3995029	17.475	0.652	3.43	0.60
V55*	21:30:02.70	12:09:43.9	0.7485716	18.110	1.138	3.61	0.59
V56	21:30:02.15	12:10:03.7	0.5703183	16.188	0.504	2.77	0.40
V57	21:30:03.35	12:09:07.9	0.3492579	17.480	1.143	4.90	0.08
V58*	21:29:54.46	12:10:10.6	0.4071922	17.519	0.649	3.07	0.52
V61	21:29:53.67	12:09:20.6	0.3996260	17.635	0.919	4.24	0.22
V62*	21:29:53.35	12:10:40.8	0.3772887	17.388	0.873	4.72	0.66
V64*	21:29:55.08	12:10:21.9	0.3642009	17.338	0.864	3.75	0.78
V65	21:29:51.28	12:09:23.3	0.7181118	17.870	1.198	4.01	0.48
V66	21:29:53.61	12:08:10.1	0.3793565	17.553	0.788	4.86	0.38
V67	21:29:52.35	12:09:51.8	0.3674503	17.824	1.069	5.53	-0.25
V69	21:29:55.79	12:09:35.9	0.5869104	18.103	1.266	2.32	-0.19
V70*	21:29:55.92	12:09:42.9	0.3676001	17.083	0.580	2.91	1.09
V71*	21:29:55.92	12:09:50.3	0.3741176	16.891	0.457	1.60	2.08
V74	21:30:00.84	12:08:37.0	0.2960204	17.430	1.159	5.28	0.23
V78	21:29:57.69	12:10:50.0	0.6646888	16.111	0.411	2.94	0.41
V80	21:29:55.00	12:09:36.2	0.6640881	16.318	0.404	2.44	0.43
V88*	21:29:58.38	12:10:29.2	0.6835572	16.350	0.758	2.02	1.87
V96	21:30:09.40	12:13:38.1	0.3963543	17.874	0.706	4.93	0.32
V97	21:29:52.82	12:10:30.9	0.6963688	17.953	1.210	3.77	0.28
V99	21:30:00.30	12:13:15.1	0.2908204	17.330	0.370	4.09	0.15
V100*	21:29:59.26	12:09:23.7	0.4063688	16.962	0.451	2.29	1.25

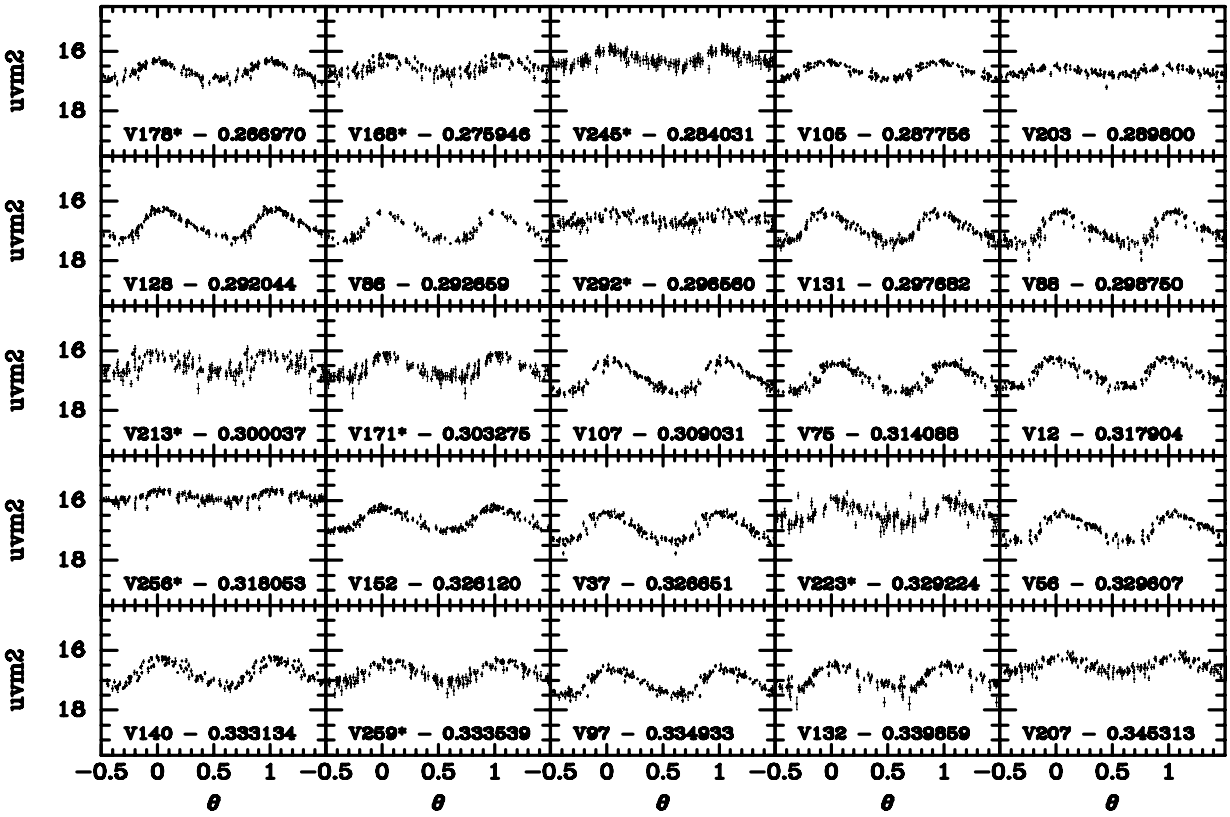

Fig. 3.— *uvm*2 light curves for the 199 RR Lyrae stars identified from the Swift data of the globular cluster M 3. Stars marked with asterisks represent those with SHARP values greater than 0.5. These are stars that are mostly in the core of M 3, identified as potential variable stars from the C01 catalog. They are likely blends, with concomitant elevated magnitudes and dampened pulsational amplitudes. They have been excluded from our detailed analysis.

2.2. Comparison to Previous Investigations

Of the 290 variable stars and variable star candidates listed in C01 for M 3, we cross-identify 217 to our UVOT data. Of these, we were able to fit periods to 201. Figure 18 compares the periods derived in this study of M 3 against those compiled in C01. As can be seen, the periods line up almost exactly, with 174 of the 201 comparisons being within .0001 days and 190 being within .001 days. Of the stars that have substantial differences in periods:

Table 3—Continued

ID (C01)	α (J2000.0)	δ	P (days)	$< uvm2 >_i$	A_{uvm2}	Var	SHARP
V102*	21:30:03.04	12:10:31.6	0.7595775	17.751	0.663	3.08	0.74
V103	21:29:41.24	12:05:27.0	0.3682380	17.542	1.112	5.56	0.08
V113	21:29:58.73	12:05:52.9	0.4059446	17.430	0.353	3.22	0.07
V114	21:29:58.13	12:10:52.2	···	16.867	···	1.72	0.20
V116*	21:29:59.34	12:09:12.8	0.6137645	17.356	1.131	3.43	0.90
V118	21:29:59.53	12:10:55.4	0.2999837	16.565	0.352	2.94	0.22
V122	21:30:15.81	12:10:26.5	···	16.680	···	1.45	0.06
V123	21:29:42.95	12:09:53.3	···	19.376	···	1.87	0.29
V124	21:29:50.12	12:06:40.4	···	19.599	···	1.72	0.42
V126	21:30:10.42	12:10:05.4	···	20.523	···	0.99	-0.26
V127	21:30:21.06	12:11:32.7	···	20.951	···	1.36	-0.05
V156	21:29:39.39	12:11:43.2	···	19.255	···	1.58	0.01
V170*	21:29:58.77	12:09:21.6	0.6779041	17.226	0.834	2.79	1.43
V182	21:30:02.87	12:10:08.8	0.3913914	17.928	1.025	4.25	-0.39

Table 4. Photometry of Variable Stars in M 3

ID	JD	$uvm2$	σ_{uvm2}
V1	2455998.8316	16.829	0.063
V1	2455999.0348	18.263	0.080
V1	2455999.0990	18.147	0.108
V1	2455999.2981	15.987	0.054
V1	2456002.9276	15.782	0.046
V1	2456006.7371	17.512	0.080
V1	2456010.7942	16.592	0.061
V1	2456010.9301	17.498	0.032
V1	2456019.3608	17.965	0.100
V1	2456022.7672	16.673	0.048

[1]Table 4 is presented in its entirety in the electronic edition of the Astronomical Journal. A portion is how here for guidance regarding its form and content.

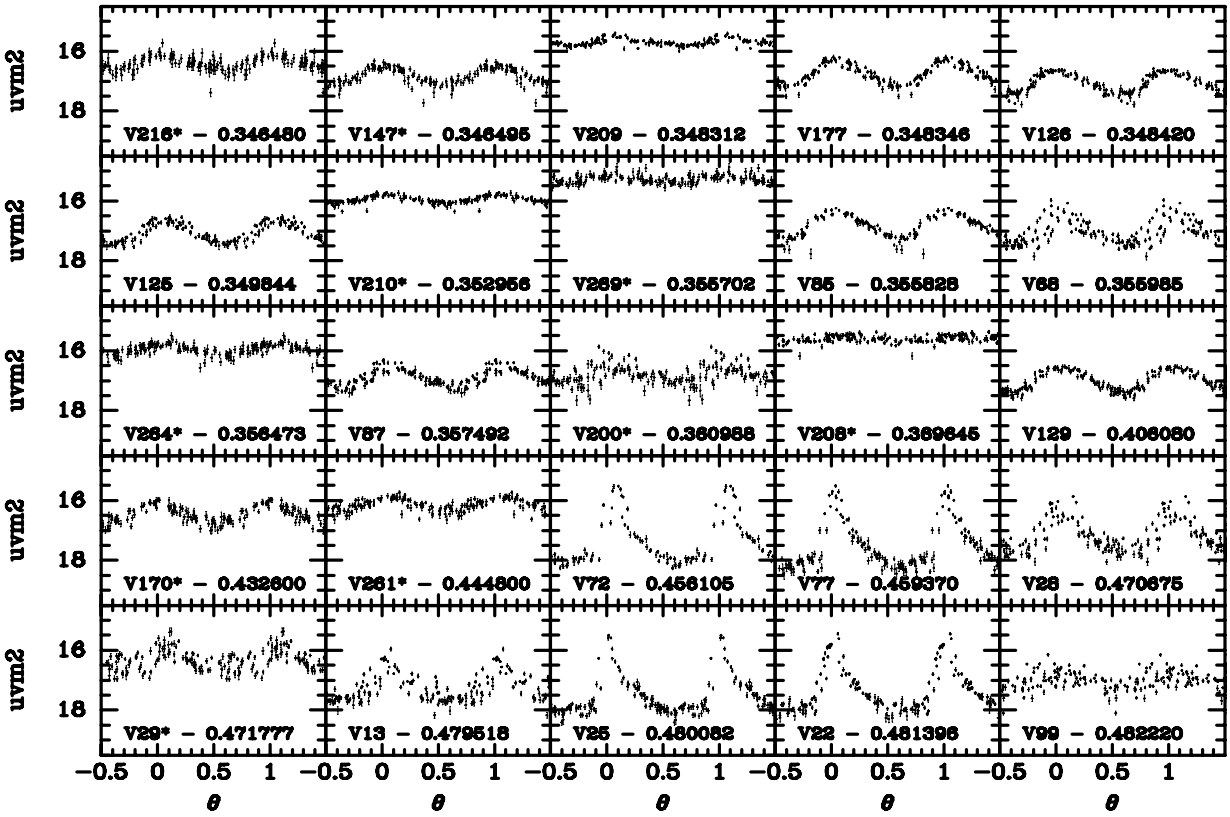

Fig. 4.— *uvm*2 light curves continued.

1. V79 and V99 have periods of 0.3581 and 0.3609 days, respectively, in C01. Our analysis finds periods of 0.4833 and 0.48222 days, respectively. Both are listed as double-mode pulsators, however and it is likely that we have measured the fundamental mode. This would be consistent with a mode ratio of 0.74-0.75 (Popielski et al. 2000).

2. V162 is listed in C01 as a non-variable star that is part of a triple system. It does show periodicity in our data (although the variability is low and the SHARP value high). We list it among the RR Lyrae stars but note that it is probably a blended multiple star system with at least one component having RR Lyrae-like pulsations. Because of its high SHARP value, it is excluded from our analysis.

3. V217 is listed in C01 as an RR Lyrae variable with no period given. Although the object has moderate variability and a high SHARP value, we do find a periodicity of 0.528 days with an RRab shaped light curve.

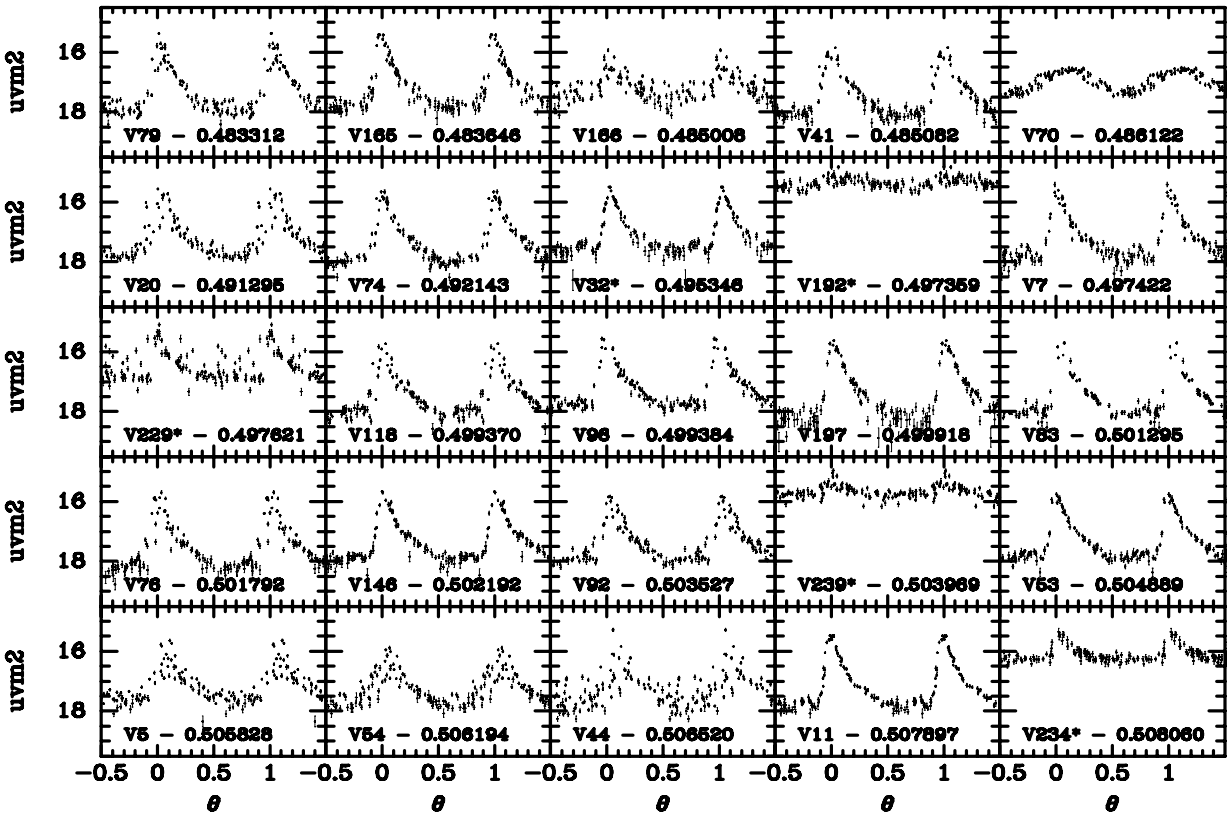

Fig. 5.— *uvm*2 light curves continued.

Of the 16 stars we match to C01 but are unable to fit periods to, none have a variability index greater than 3.0. Of these stars:

1. Six stars listed in C01 as nonvariable are confirmed as non-variable by our data.

2. Six stars listed in C01 as SX Phoenicis stars are measured as non-variable in our data. SX Phoenicis stars tend to be faint with rapid pulsations and small amplitudes. Our data are not optimized for their detection so it is not surprising that we can not confirm their variation. The only SX Phoenicis star we do confirm – V291 – has a large amplitude and was identified by *a priori* knowledge of the period.

3. V138, listed by C01 as a semi-regular variable, shows little variation in our data, with a dispersion of only 1.1 times the formal scatter. This is not surprising as these stars are very faint in the UV.

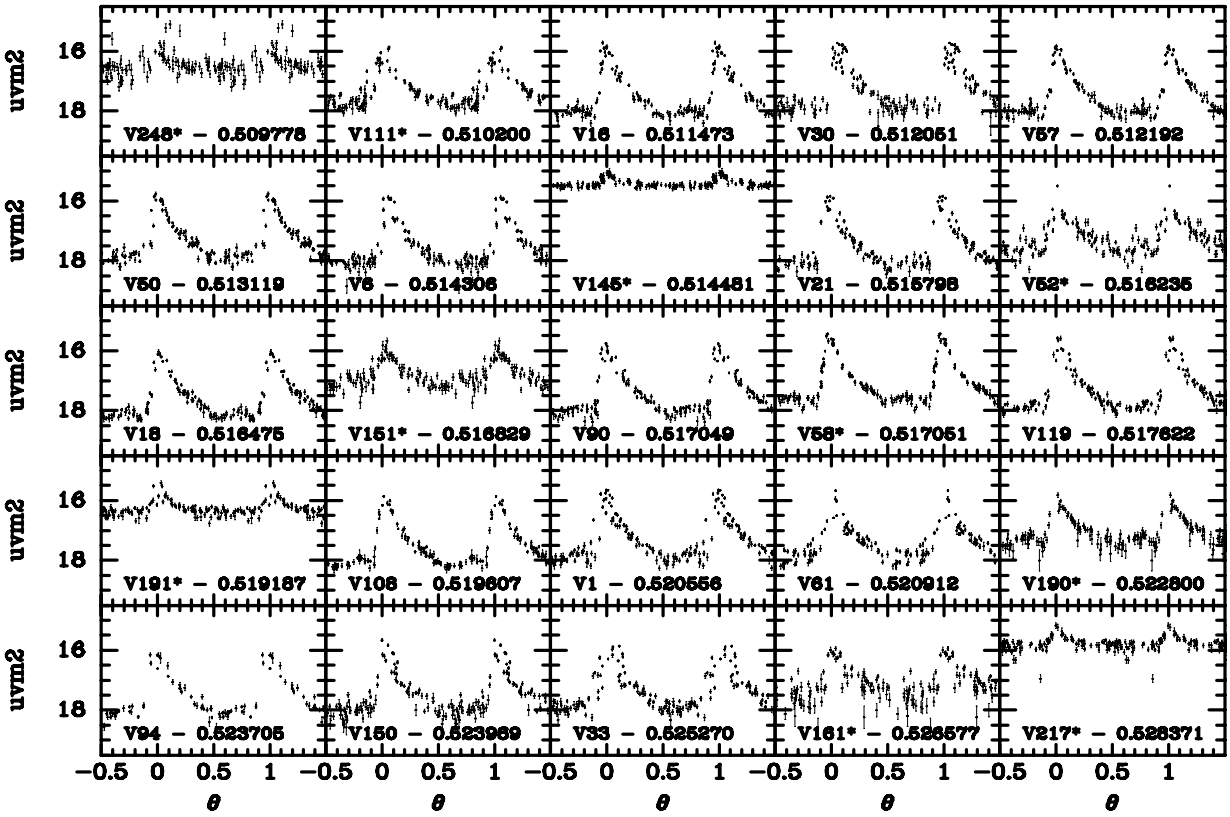

Fig. 6.— *uvm*2 light curves continued.

4. V287, which C01 are unable to classify, shows little variation in our data, with a dispersion of only 1.6 times the formal scatter

5. V290, listed in C01 as a double-mode RR Lyrae, shows no clear minimum in the phase dispersion diagram. It is possible our analysis is being confounded by the double mode.

6. V296, listed by C01 as an eclipsing binary with a period of .446 days, shows no clear minimum in the phase dispersion diagram. It does have a weak minimum on .377 day cycle.

We identify one potential new variable star in M 3 – marked as V300 in Table 2. This star shows significant variation over the course of the observing campaign with a very crude period of 253 days (see Figure 12). We note, however, that our data span just over one pulsation cycle and show multiple minima in the 200-250 day range as well as in other ranges of periodicity. If this is indeed a real variable, it could be pulsating on a much more

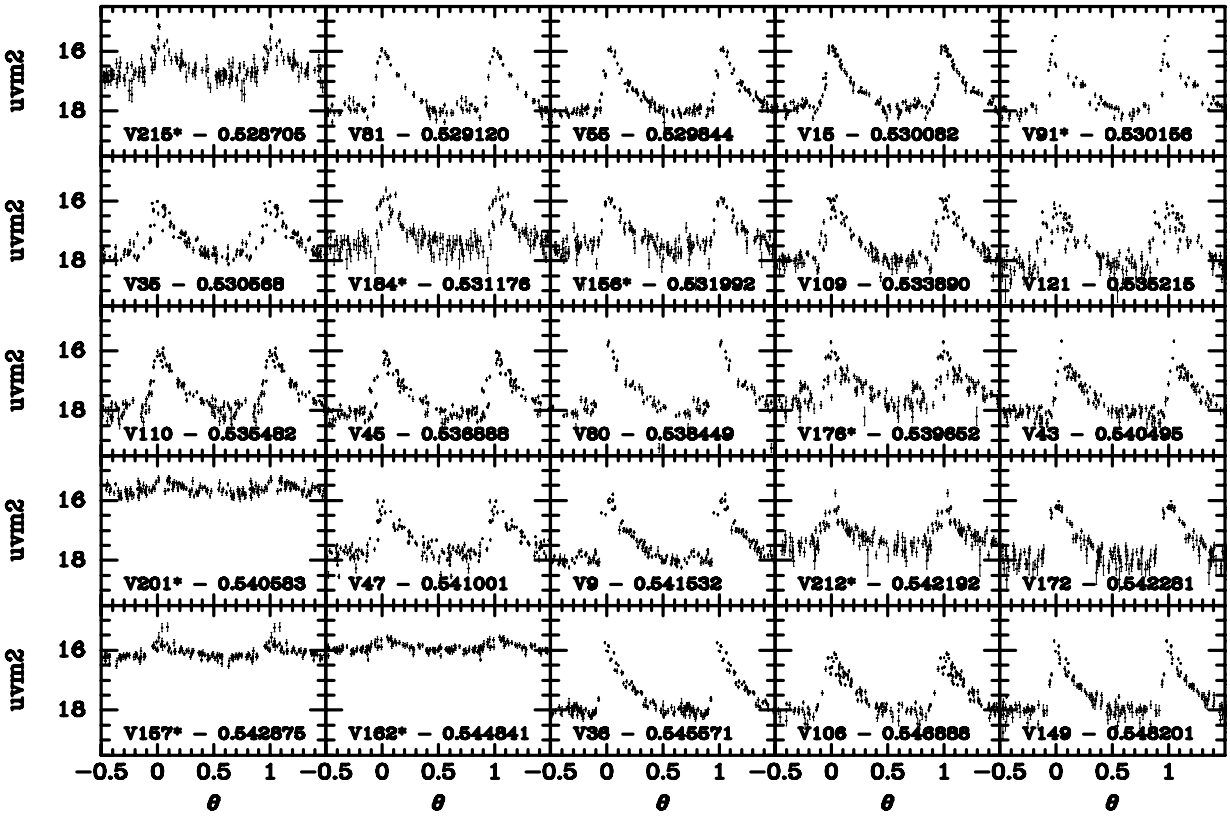

Fig. 7.— *uvm*2 light curves continued.

irregular or higher-order cycle. Further investigation is warranted.

Of the 182 variable stars and variable star candidates identified by C01 in M 15, we are able to identify counterparts to 85. Of these, we were able to fit periods to 77. Figure 19 compares the periods derived in this study of M 15 against those compiled in C01. As can be seen, the periods line up almost exactly, with 47 of the 77 comparisons being within .0001 days and 68 being within .001 days. The only star which has a significant difference in period is V34. This star is listed by C08 as a possible eclipsing binary with a period of 1.1591 days and shows a somewhat irregular light curve. We find a period of 2.037 days and show a sawtooth pattern to the light curve, which indicates that this could be an anomalous Cepheid. We also identify one new RRc star, which we label V182.

Of the eight stars we match to C01 but are unable to fit periods to, none have a variability index greater than 3.0, Of these stars:

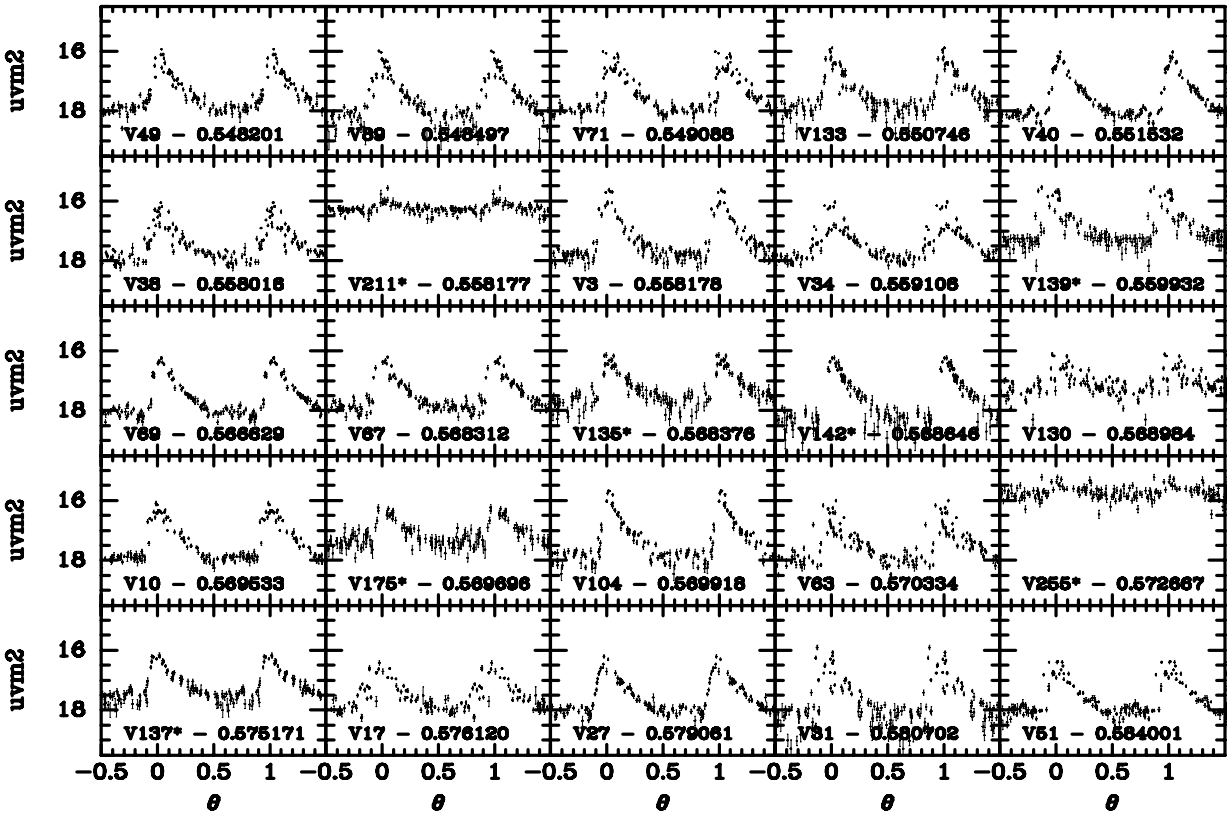

Fig. 8.— *uvm*2 light curves continued.

1. Five stars listed in C01 as of uncertain nature (V122, V123, V124, V126 and V127) show up as non-variable in our data. We note that these stars are faint and have small amplitudes.

2. V27 is listed as non-variable and we confirm this, measure a dispersion of 1.33 times the formal error.

3. We do not detect any variability in the SX Phoenicis star V156 to a limit of 1.56 times the formal error. This is not surprising given its faintness and small amplitude.

4. The RR Lyrae variable V114 has C01 position that lies between two point source in our data. Neither shows significant variability.

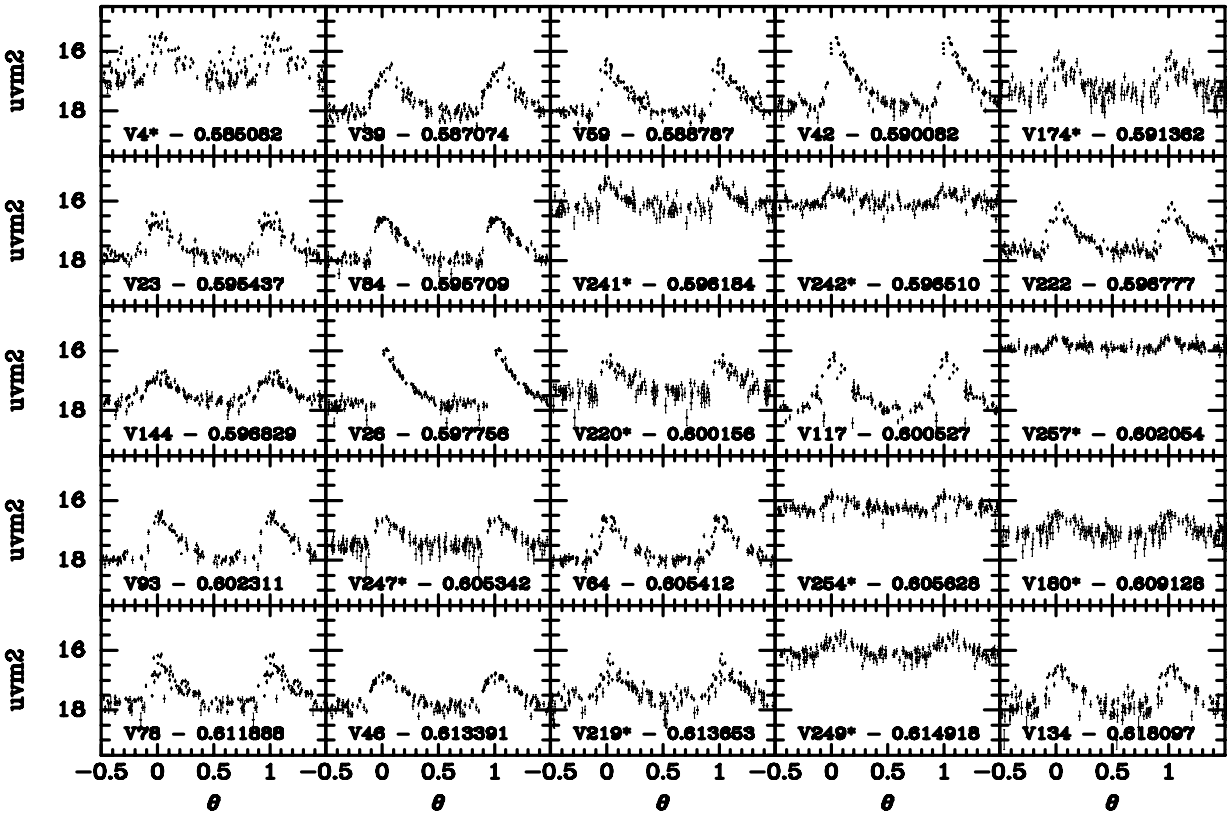

Fig. 9.— *uvm*2 light curves continued.

3. Analysis

3.1. RR Lyrae Star Pulsational Properties

Figure 20 compares the *uvm*2 amplitudes with SHARP values less than 0.5 to the *V*-band amplitudes compiled in C01 (top). The top panel shows 130 RR Lyrae variable stars in M3 while the bottom shows 58 from M15. As can be seen, the pulsational amplitudes in the UV are substantially larger, with an average A_{uvm2}/A_V ratio of 1.84±0.41 in M3 and 1.70±0.46 in M15. The large NUV amplitudes are expected, given both previous investigations and the astrophysical properties of RR Lyrae stars, which pulsate over a temperature range where the UV flux can increase dramatically. This ratio appears to be constant with pulsational period.

Figure 21 shows the *uvm*2 Bailey (1919) diagram for both clusters. Large diamonds mark the known double-mode pulsators in M 3 while large squares mark those in M 15.

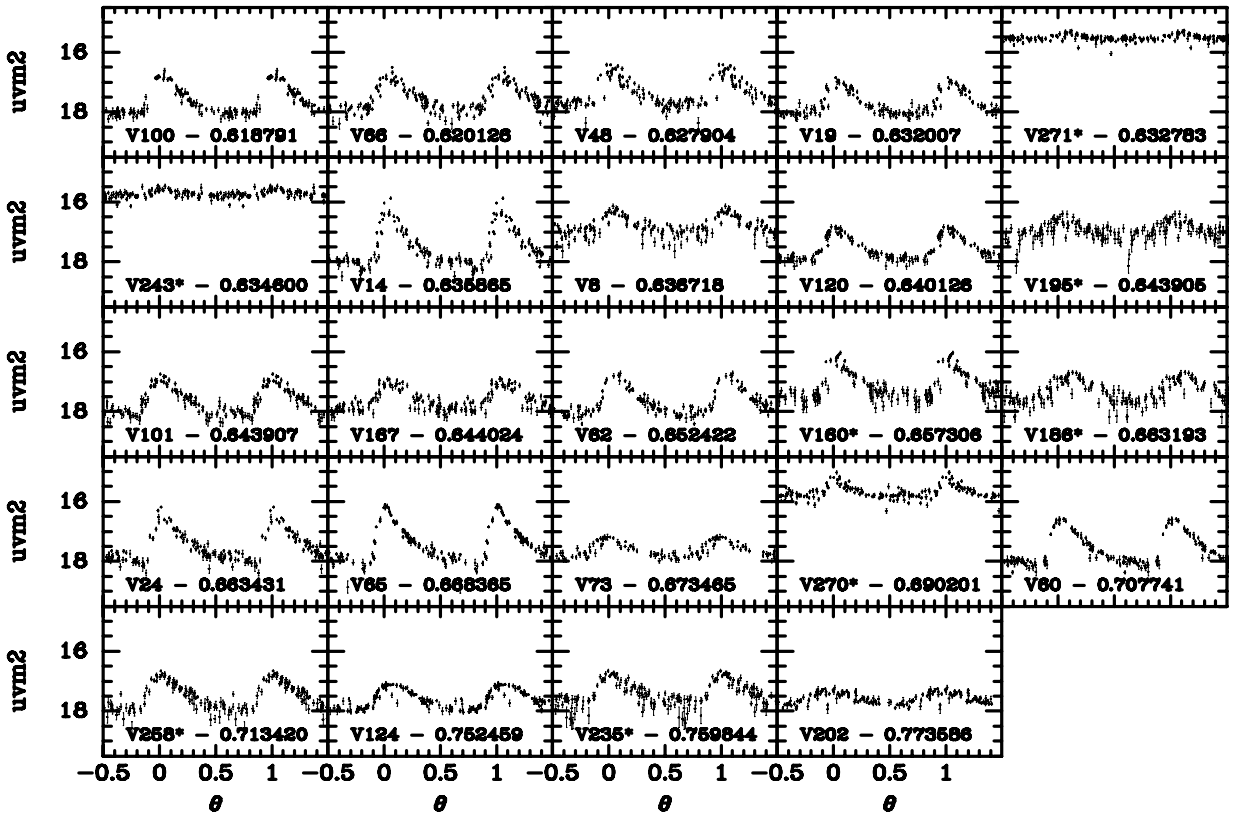

Fig. 10.— $uvm2$ light curves continued.

The familiar loci of RRab stars (the diagonal sequences at long periods) and RRc stars (the relatively flatter trend at shorter periods) are plainly visible. We have overlayed fits to the trends of stars in M 3 (solid) and M 15 (dashed) to draw the eye to these sequences. The comparison between M 3 and M 15 provides an excellent illustration of the Oosterhoff effect. Compared to the RR Lyrae stars in M 3, those of M 15 are at longer periods, in both fundamental and first overtone. M 15 also shows a much larger proportion of first overtone pulsators.

Both clusters' RRab stars follow a linear log P-A_{uvm2} sequence, although M 15's RRab show a much shallower slope. There have been indications that the RRab locus is slightly curved, but we do not show this clearly in our data. Interestingly, the RRc stars show a rough diagonal sequence or possibly even a parabola. This has been hinted at before in RR Lyrae data (see, for example, the compilation of Bailey diagrams in Smith et al. 2011) and has been predicted based on theoretical models (see, e.g. Bono et al. 1997). In this scenario, pulsational amplitude linearly tracks temperature for fundamental pulsators but

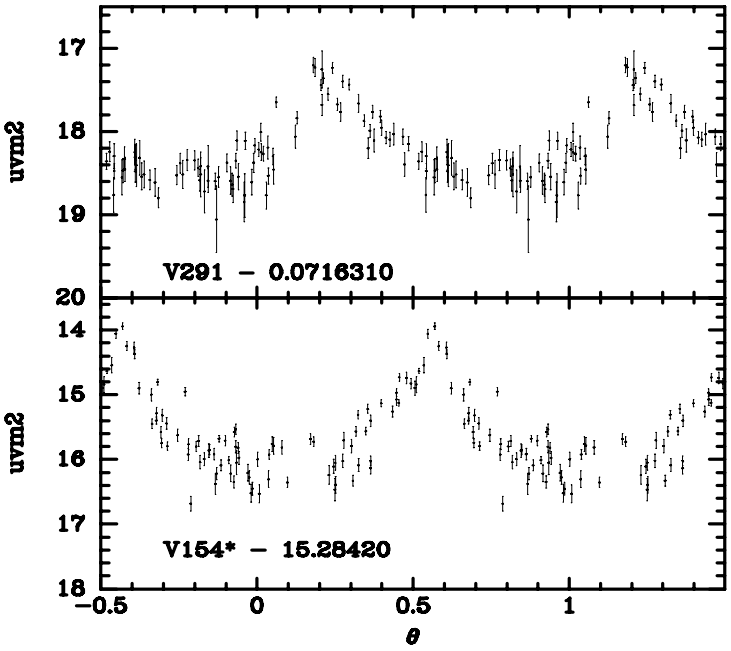

Fig. 11.— $uvm2$ light curves for the SX Phoenicis star V291 (top) and the classical Cepheid V154 (bottom) in the globular cluster M 3.

tracks it non-linearly for first overtone pulsators, creating the parabola shape. M 3's RRc log P-A_{uvm2} sequence is consistent with a parabola. However, the RRc stars would also be consistent with a linear slope or a constant value. By constrast, M 15's more numerous RRc stars show a distinct parabola shape, with a log P-A_{uvm2} sequence that is not consistent with either a linear slope or a flat trend. This suggests that NUV surveys of other clusters, especially OoII clusters, could provide a unique test of theoretical models of first overtone pulsators.

One of the fundamental measures used to study RRab stars is period shift – the displacement of RRab stars to longer periods at equal amplitudes in comparison to a reference population (Sandage 1982a, 1982b; Carney et al. 1992). Star of equal amplitude have similar effective temperatures (Sandage et al. 1981) so an increase in period at a fixed amplitude is likely due to increased luminosity, according to the pulsation equation of van Albada & Baker (1971). The period shift is postulated to arise from differences in metallicity (see, e.g.,

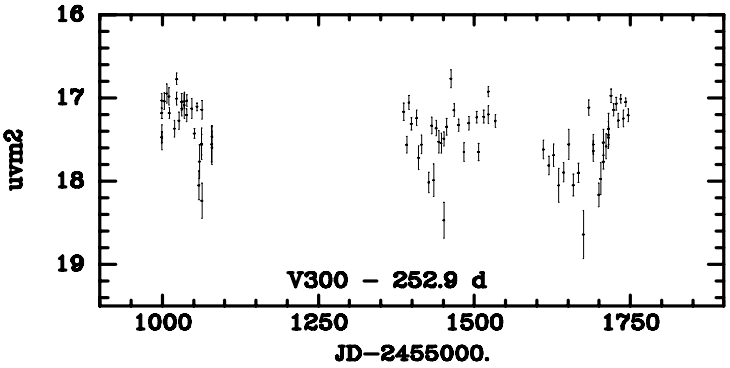

Fig. 12.— $uvm2$ light curve for a possible long-term or irregular variable discovered in M 3.

Sandage et al. 1981) although other studies have indicated that Oosterhoff type can play a critical role (see, e.g., Bono et al. 2007). A fuller discussion of this debate can be found in Smith et al. (2011).

M 3 is the usual reference population used to measure period shift. We define the fundamental RRab sequence in UVOT magnitudes as:

$$A_{uvm2} = -0.407 - 8.85\times \log P$$

The slope of this relation between amplitude and period is steeper in $uvm2$ compared to optical passbands (see, e.g., Siegel & Majewski 2000, where the period shift slope for M 3 is calculated as 7.75 and 6.41 in the B and V bands, respectively). This confirms that the $uvm2$ amplitudes are more sensitive to pulsational period (and thus, effective temperature) than the optical passbands.

We define the period shift from this relation as:

$$\Delta \log P = -(0.0460 + 0.113 A_{uvm2} + \log P)$$

Figure 22 shows the period-shift of the RRab stars in both clusters. The M3 RRab stars cluster around the origin with a median $\Delta \log P$ of 0.000, which is expected since they define the period shift. The M15 RRab stars show a median period shift of -0.008, although it is weaker for the shorter-period stars (as hinted at by the shallower slope of the RRab sequence in Figure 21). This confirms that the period shift seen in Figure 21 is real but suggests that further investigation is warranted to confirm that the period-shift separation between OoI and OoII is as clean in the NUV as it is in the optical passbands.

3.2. RR Lyrae Star Temperatures and Surface Gravities

The physical properties of the RR Lyrae stars in M 3 and M 15 have been explored in exhaustive detail by previous investigations. We do wish to revisit one aspect of the RR Lyrae stars to highlight something unique in the NUV data: a strong sensitivity to both temperature and surface gravity.

There are a variety of diagnostics that can measure the temperatures of RR Lyrae stars. CCC05 list six different methods that they use to measure temperatures for 133 RR Lyrae variable stars in M 3, providing a very through investigation of RR Lyrae star temperatures.

Figure 23 compares the temperatures CCC05 calculate from $B-V$ photometry and the temperature scale of Sekiguchi & Fukugita (2000) to three different photometric indices: the $B-V$ colors used in that study and $uvm2-B$ and $uvm2-V$ indices derived by combining our photometry with that of CCC05. We attempted a comparison to UVOT colors but the $uvw1$ and $uvw2$ passbands had too few observations to derive useful mean magnitudes for the RR Lyrae.

Overlaid on the panels are predicted theoretical colors as a function of T_{eff} for a range of surface gravities. The theoretical colors were derived from the models of Castelli & Kurucz (2003) using a metallicity of [Fe/H]=-1.5, an α-abundance of $[\alpha/Fe]$=+0.4 and microturbulent velocity of $v_{turb} = 2.0$ km s^{-1}. The theoretical magnitudes were corrected for reddening of $E(B-V) = 0.01$, using the non-linear corrections for the $uvm2$ photometry discussed in the Appendix of Paper I.

The top panel of Figure 23 shows the CCC05 colors compared to the theoretical temperatures. They obviously track well, given that the latter was derived from the former. Note, that the broadband photometry is relatively insensitive to the surface gravity. The lines for *log g* values from 2.0 to 3.5 bunch very closely together.

The two lower panels of Figure 23 show the combination of CCC05 photometry and $uvm2$ photometry. These hybrid UV-optical colors are far more sensitive to the surface gravity. This is expected, given that the combination of optical and UV filters straddles the Balmer jump, the strength of which is highly sensitive to surface gravity in moderate to hot stars. We see that that while the cooler stars have inferred surface gravities in the range of $log\ g$ 2.0 to 2.5, the hotter stars have surface gravities of nearly 3.0.

This is roughly consistent with both observational data and theoretical expectations. CCC05 calculate $log\ g$ from the equation of stellar structure and show a steady increase with effective temperature from $log\ g \sim 2.7$ to $log\ g \sim 3.0$. We generated a synthetic horizontal branch for M 3 using the online tool of Dotter et al. (2008) and assuming [Fe/H]=-1.5, [α/Fe]=+0.2 and an average mass of 0.8 $M_{\odot}$. The model shows surface gravity gradually increasing with temperature over the range of RR Lyrae stars from $log\ g = 2.67$ at $log(T_{eff}) = 3.78$ to $log\ g = 3.11$ at $log(T_{eff}) = 3.88$.

Our analysis shows the cooler RRab stars having slightly lower surface gravities than expected by about 0.5 dex. This is likely due to our use of intensity-weighted mean magnitudes which are, at best, an approximation of the static color an RR Lyrae star would have if it were not pulsating. Bono et al. (1995) showed that colors derived from intensity weighted magnitudes are systematically offset from the static-star colors, owing to the effect of increasing amplitude. They compile a table of corrections to be applied to $B-V$ colors for fundamental and first overtone colors. It is not clear how these would scale to the UV and deriving these corrections is beyond the scope of the current study. However, the discrepancy between the models and the data in Figure 23 indicates that this correction is likely to be significant (several tenths of a magnitude) and that further investigation is critical if we are to derive fundamental stellar parameters from NUV-optical photometry.

The dual sensitivity of the NUV photometry to both temperature and surface gravity provides a unique window into the astrophysics of pulsating stars. By comparing an index that is not sensitive to surface gravity (such as $B-V$) to one that is ($uvm2-B$ or $uvm2-V$), we can simultaneously measure both properties from photometry alone. Our M 3 results demonstrate that this can be done and that is it roughly consistent with theoretical expectations and previous observational analysis. This will be a powerful tool for future investigations into other populations of RR Lyrae stars.

3.3. RR Lyrae Star Period-Luminosity Relationship

The diagonal HB seen in Figures 1 and 2 would suggest a potential period-luminosity relationship for RR Lyrae stars in the NUV. The top panel of figure 24 shows the period-magnitude relation for both clusters and appears to confirm this supposition. The stars follow a sequence of increasing magnitude with period for both populations.

Two of M 3's stars are substantially brighter than the period-luminosity relationship by more than half a magnitude. This might suggest they are foreground or evolved objects but their V and B magnitudes in C01 are well within the primary sequence. Although their SHARP values are below 0.5, they are slightly high (~ 0.3) and their amplitudes are a bit low compared to stars of similar period. This suggests they may be blends. Removing these two stars for consideration, we find a linear fit to the period-magnitude sequence of:

$$uvm2 = 18.06 + 2.41\times \log P$$

Correcting for the distance modulus and reddening listed in Harris (1996) yields:

$$M_{uvm2} = 2.93 + 2.41\times \log P$$

M 15 has five stars that are outliers by more than half a magnitude on the period-luminosity relationship, all of which have elevated SHARP values (0.22-0.43). Removing these from the fit yields:

$$uvm2 = 18.18 + 1.42\times \log P$$

Correcting for the distance modulus and reddening listed in Harris (1996) yields:

$$M_{uvm2} = 2.25 + 1.42\times \log P$$

The bottom panel of Figure 24 shows the stars from both M 3 and M 15, corrected for the distances modulus and foreground reddening values listed in Harris (1996). As can be seen, the RR Lyrae in M 15 are brighter than those of comparable period in M3. There is some scatter and non-linearity in the comparison, with the coolest RRab stars being almost half a magnitude brighter while the hottest RRc stars are a few tenths of a magnitude brighter (as implied by the different slopes in the period-magnitude relations of the two clusters). The difference is dependent on the assumed reddening (for most of the RR Lyrae temperature

range, the extinction in $uvm2$ is greater than 8.0). However, even modulo reddening, this comparison suggests that the NUV period-luminosity relationship has a strong metallicity dependence, far stronger than is seen in the IR, where the metallicity dependence is a few hundredths of a magnitude to a few tenths of a magnitude (Bono et al. 2001; Sollima et al. 2006; Muraveva et al. 2015). Alternatively, the different slope in the period-magnitude relationships could indicate that the relationship changes depending on Oosterhoff type.

As simple fit with a cross-term to these two trends yields the relation:

$$M_{uvm2} = 4.103 + 0.782\ [\mathrm{Fe/H}] + 4.117\ \log P + 1.138\ \log P\ [\mathrm{Fe/H}]$$

confirming both the strong metallicity dependence and the non-linearity. However, this "fit" is based on two clusters. Many more clusters are needed to determine if the period-magnitude-metallicity relationship varies smoothly with metallicity or is different for the different Oosterhooff classifications. It would also be useful to study objects that have a range of metallicities, such as the Magellanic Clouds or Omega Centauri, so that distance and reddening differences can be minimized. The most robust evaluation would come from studying RR Lyrae with trigonometric parallaxes, such as those expected to emerge from the GAIA mission.

4. Conclusions

We have presented the first thorough investigation into the NUV pulsational properties of variable stars in the well-studied globular clusters M 3 and M 15. We cross-identify and fit periods to 201 variable stars in M 3 and 85 in M 15. Of these 286 stars, 282 are RR Lyrae stars. The remainder are three Cepheids and one SX Phoenicis star. We identify one potential new variable in M 3 and one new RRc star in M 15.

We find that the RR Lyrae stars have, as expected, very large NUV amplitudes compared to the optical and infrared, with value ranging up to 2.7 magnitudes. We find that the RR Lyrae conform to the same paradigms established in the optical, exhibiting a clear Oosterhoff effect, a period shift between M 3 and M 15 and a correlation between temperature and pulsational amplitude. We show that the combination of NUV and optical data shows remarkable sensitivity to both the temperature and surface gravity of the RR Lyrae stars, although our comparison to the Kurucz models underestimates the surface gravity of the cooler RRab stars likely due to the effect of the large amplitudes on the intensity-weighted $uvm2 - B$ and $uvm2 - V$ colors.

We further find that the stars exhibit a clear period-magnitude relation in the NUV. While we only have two cluster to compare, the difference between them suggests that the period-lumonisity relationship has a strong and possibly non-linear dependence on metallicity.

Swift continues to observe Galactic clusters that are known to host populations of RR Lyrae, both as part of our ongoing investigation and as part of routine monitoring of X-ray transients in globular clusters (Bahramian et al. 2013). This will enable more through explorations of the interaction of RR Lyrae pulsational properties, metallicity and reddening.

The authors acknowledge sponsorship at PSU by NASA contract NAS5-00136. This research was also supported by the Swift Guest Investigator Program through NASA grant NNX14AC31G. The authors thank Caryl Gronwall for useful comments and the anonymous referee for useful corrections. The Institute for Gravitation and the Cosmos is supported by the Eberly College of Science and the Office of the Senior Vice President for Research at the Pennsylvania State University.

REFERENCES

Bahramian, A., Heinke, C. O., Sivakoff, G. R., Altamirano, D., & Wijnands, R. 2013, The Astronomer's Telegram, 5396, 1

Bailey, S. I., Leland, E. F., Woods, I. E., & Pickering, E. C. 1919, Annals of Harvard College Observatory, 78, 195

Baker, R. H., & Baker, H. V. 1956, AJ, 61, 283

Bakos, G. A., Benko, J. M., & Jurcsik, J. 2000, Acta Astron., 50, 221

Benkő, J. M., Bakos, G. Á., & Nuspl, J. 2006, MNRAS, 372, 1657

Bingham, E. A., Cacciari, C., Dickens, R. J., & Pecci, F. F. 1984, MNRAS, 209, 765

Blazhko, S. 1907, *Astron. Nachr.*, 175, 325

Bonnell, J., Wu, C.-C., Bell, R. A., & Hutchinson, J. L. 1982, PASP, 94, 910

Bono, G., Caputo, F., & Stellingwerf, R. F. 1995, ApJS, 99, 263

Bono, G., Caputo, F., Castellani, V., & Marconi, M. 1997, A&AS, 121, 327

Bono, G., Caputo, F., Castellani, V., Marconi, M., & Storm, J. 2001, MNRAS, 326, 1183

Bono, G., Caputo, F., & Di Criscienzo, M. 2007, A&A, 476, 779

Breeveld, A. A., et al. 2010, MNRAS, 874

Breeveld, A. A., Landsman, W., Holland, S. T., et al. 2011, American Institute of Physics Conference Series, 1358, 373

Burrows, D. N., et al. 2005, Space Science Reviews, 120, 165

Butler, R. F., Shearer, A., Redfern, R. M., et al. 1998, MNRAS, 296, 379

Cacciari, C., Corwin, T. M., & Carney, B. W. 2005, AJ, 129, 267 [CCC05]

Carney, B. W., Storm, J., & Jones, R. V. 1992, ApJ, 386, 663

Carretta, E., Cacciari, C., Ferraro, F. R., Fusi Pecci, F., & Tessicini, G. 1998, MNRAS, 298, 1005

Castelli, F., & Kurucz, R. L. 2003, Modelling of Stellar Atmospheres, 210, 20P

Clement, C. M., Muzzin, A., Dufton, Q., et al. 2001, AJ, 122, 2587 [C01]

Corwin, T. M., & Carney, B. W. 2001, AJ, 122, 3183 [CC)1]

Corwin, T. M., Borissova, J., Stetson, P. B., et al. 2008, AJ, 135, 1459 [C08]

Del Principe, M., Piersimoni, A. M., Bono, G., et al. 2005, AJ, 129, 2714

Dieball, A., Knigge, C., Zurek, D. R., et al. 2007, ApJ, 670, 379

Dotter, A., Chaboyer, B., Jevremović, D., et al. 2008, ApJS, 178, 89

Downes, R. A., Margon, B., Homer, L., & Anderson, S. F. 2004, AJ, 128, 2288

Ferraro, F. R., & Paresce, F. 1993, AJ, 106, 154

Filippenko, A. V., & Simon, R. S. 1981, AJ, 86, 671

Gehrels, N., et al. 2004, ApJ, 611, 1005

Guhathakurta, P., Yanny, B., Bahcall, J. N., & Schneider, D. P. 1994, AJ, 108, 1786

Hardie, R. H. 1955, ApJ, 122, 256

Harris, W. E. 1996, AJ, 112, 1487

Hartman, J. D., Kaluzny, J., Szentgyorgyi, A., & Stanek, K. Z. 2005, AJ, 129, 1596

Hutchinson, J. L., Lillie, C. F., & Hill, S. J. 1977, ApJ, 211, 207

Kaluzny, J., Hilditch, R. W., Clement, C., & Rucinski, S. M. 1998, MNRAS, 296, 347

Kovács, G., & Kupi, G. 2007, A&A, 462, 1007

Layden, A. C. 1998, AJ, 115, 193

Muraveva, T., Palmer, M., Clementini, G., et al. 2015, ApJ, 807, 127

Neeley, J. R., Marengo, M., Bono, G., et al. 2015, ApJ, 808, 11

Oosterhoff, P. T. 1939, The Observatory, 62, 104

Pei, Y. C., 1992, ApJ, 395, 130

Poole, T. S., et al. 2008, MNRAS, 383, 627

Popielski, B. L., Dziembowski, W. A., & Cassisi, S. 2000, Acta Astron., 50, 491

Roming, P. W., Townsley, L. K., Nousek, J. A., et al. 2000, Proc. SPIE, 4140, 76

Roming, P. W. A., Hunsberger, S. D., Mason, K. O., et al. 2004, Proc. SPIE, 5165, 262

Roming, P. W. A., et al. 2005, Space Science Reviews, 120, 95

Rosino, L. 1950, ApJ, 112, 221

Rosino, L. 1969, Information Bulletin on Variable Stars, 327, 1

Sandage, A., Katem, B., & Sandage, M. 1981, ApJS, 46, 41

Sandage, A. 1982, ApJ, 252, 553

Sandage, A. 1982, ApJ, 252, 574

Sandquist, E. L., Gordon, M., Levine, D., & Bolte, M. 2010, AJ, 139, 2374

Schiavon, R. P., Dalessandro, E., Sohn, S. T., et al. 2012, AJ, 143, 121

Sekiguchi, M., & Fukugita, M. 2000, AJ, 120, 1072

Siegel, M. H., Porterfield, B. L., Linevsky, J. S., et al. 2014, AJ, 148, 131 [Paper I]

Siegel, M. H., & Majewski, S. R. 2000, AJ, 120, 284

Silbermann, N. A., & Smith, H. A. 1995, AJ, 110, 704

Smith, H. A. 1995, Science, 270, 1236

Smith, H. A., Catelan, M., & Kuehn, C. 2011, RR Lyrae Stars, Metal-Poor Stars, and the Galaxy, 17

Sollima, A., Cacciari, C., & Valenti, E. 2006, MNRAS, 372, 1675

Stetson, P. B. 1987, PASP, 99, 191

Stetson, P. B. 1994, PASP, 106, 250

Thomson, G. S., Dieball, A., Knigge, C., Long, K. S., & Zurek, D. R. 2010, MNRAS, 406, 1084

Tuairisg, S. Ó., Butler, R. F., Shearer, A., et al. 2003, MNRAS, 345, 960

van Albada, T.S. & Baker, N. 1971, ApJ, 169, 311

Wheatley, J. M., Welsh, B. Y., Siegmund, O. H. W., et al. 2005, ApJ, 619, L123

Wheatley, J., Welsh, B. Y., & Browne, S. E. 2012, PASP, 124, 552

Yang, S.-C., & Sarajedini, A. 2012, MNRAS, 419, 1362

Zheleznyak, A. P., & Kravtsov, V. V. 2003, Astronomy Letters, 29, 599 Query Results from the ADS Database

Table 5. Photometry of Variable Stars in M 15

ID	JD	$uvm2$	σ_{uvm2}
V1	2455702.9226	16.927	0.069
V1	2456403.3904	17.677	0.071
V1	2456410.6693	17.604	0.052
V1	2456419.4170	17.874	0.059
V1	2456426.6931	18.104	0.076
V1	2456434.7068	16.605	0.042
V1	2456439.0323	16.641	0.048
V1	2456450.9921	17.702	0.092
V1	2456459.2694	17.106	0.056
V1	2456467.0026	17.948	0.072

[1]Table 5 is presented in its entirety in the electronic edition of the Astronomical Journal. A portion is how here for guidance regarding its form and content.

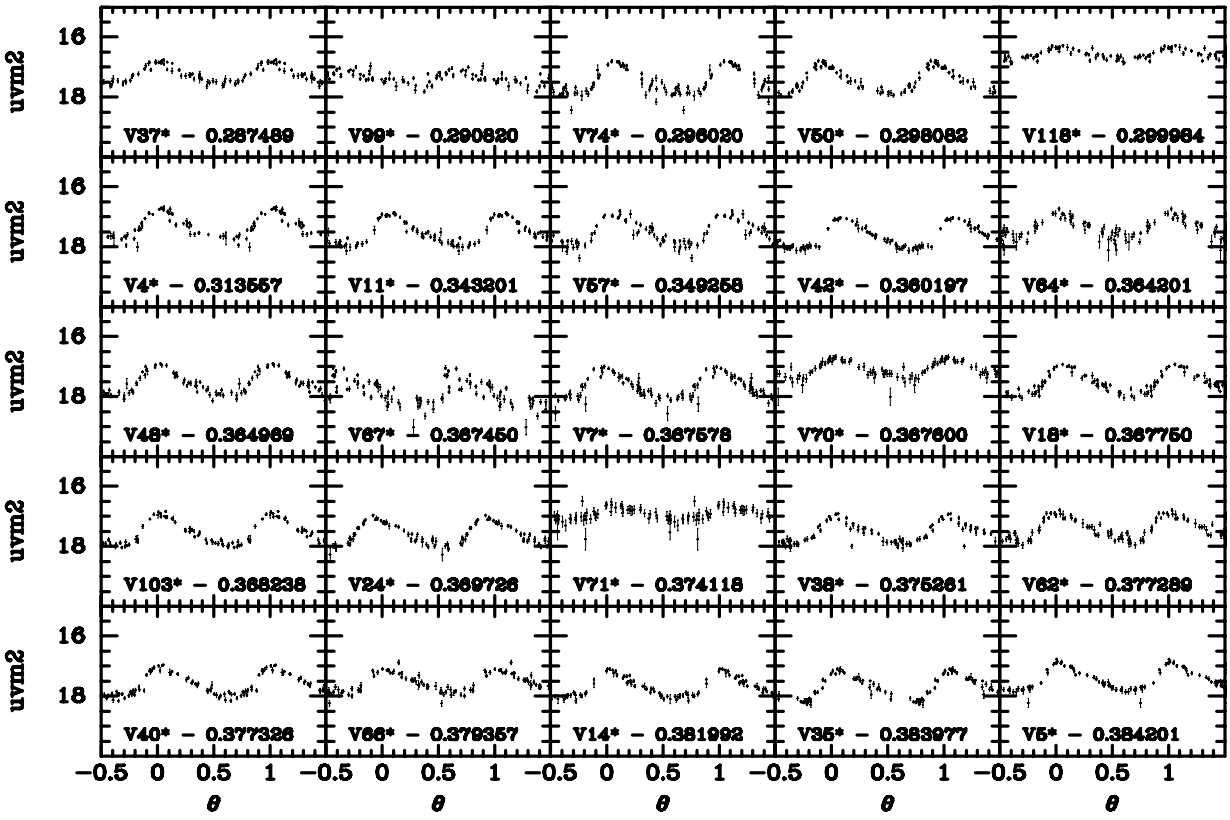

Fig. 13.— *uvm*2 light curves for the 76 RR Lyrae stars identified from the Swift data of the globular cluster M 15. Stars marked with asterisks represent those with SHARP values greater than 0.5. These are stars that are mostly in the core of M 15, identified as potential variable stars from the C01 catalog. They are likely blends, with concomittant elevated magnitudes and dampened pulsational amplitudes. They have been excluded from our detailed analysis.

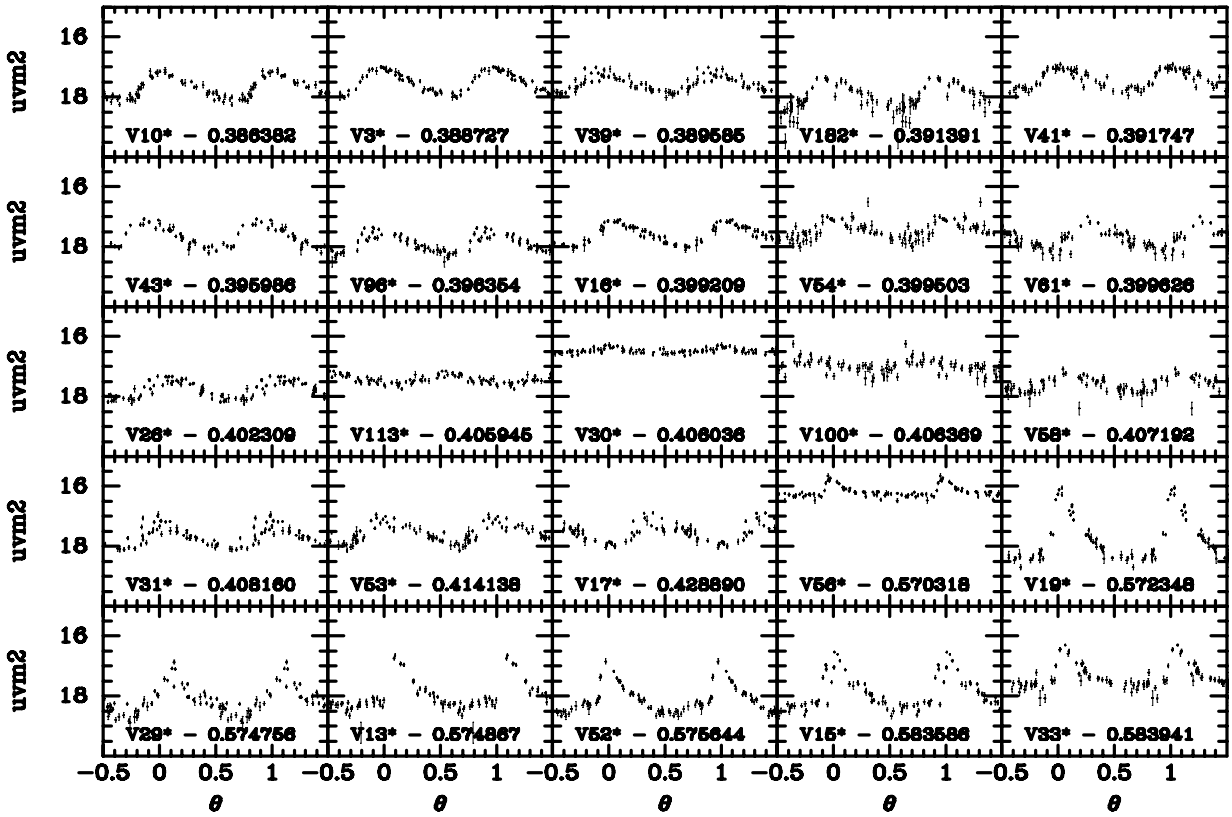

Fig. 14.— $uvm2$ light curves continued.

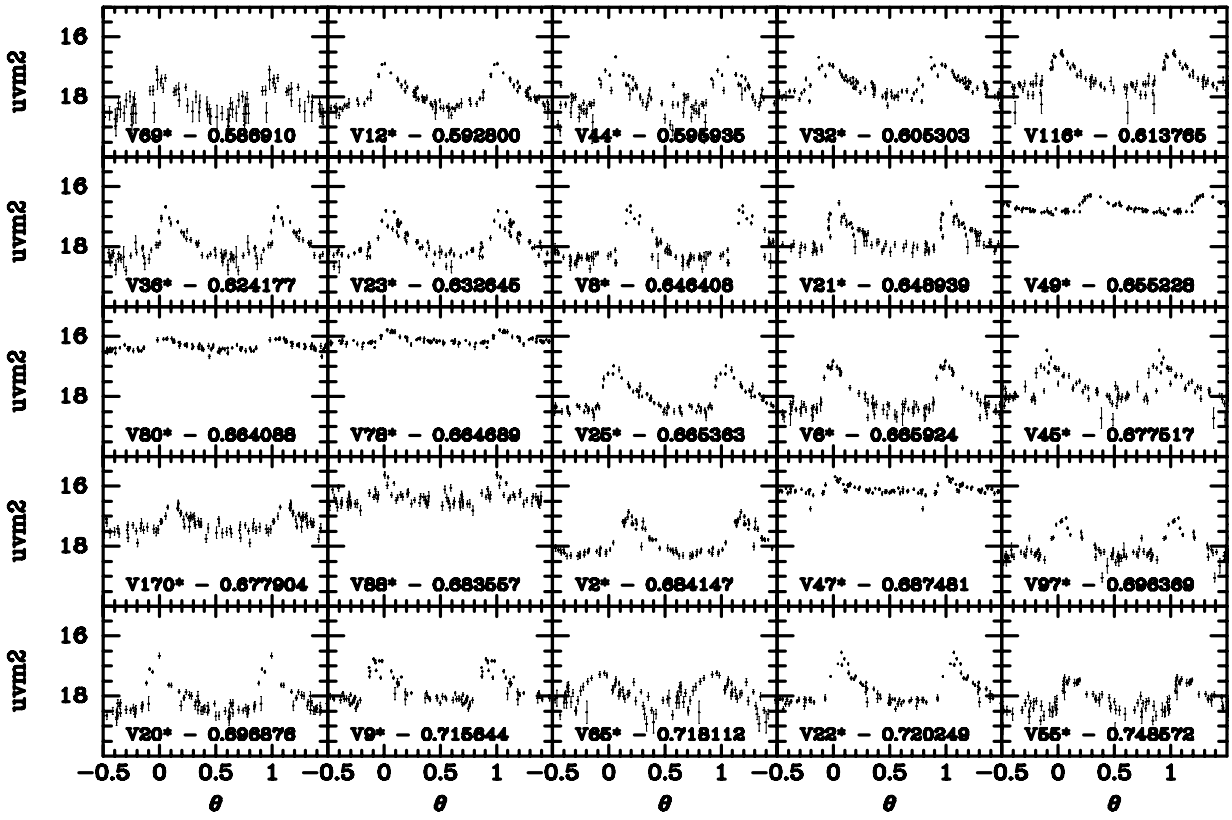

Fig. 15.— $uvm2$ light curves continued.

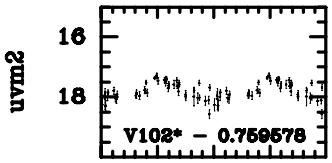

Fig. 16.— $uvm2$ light curves continued.

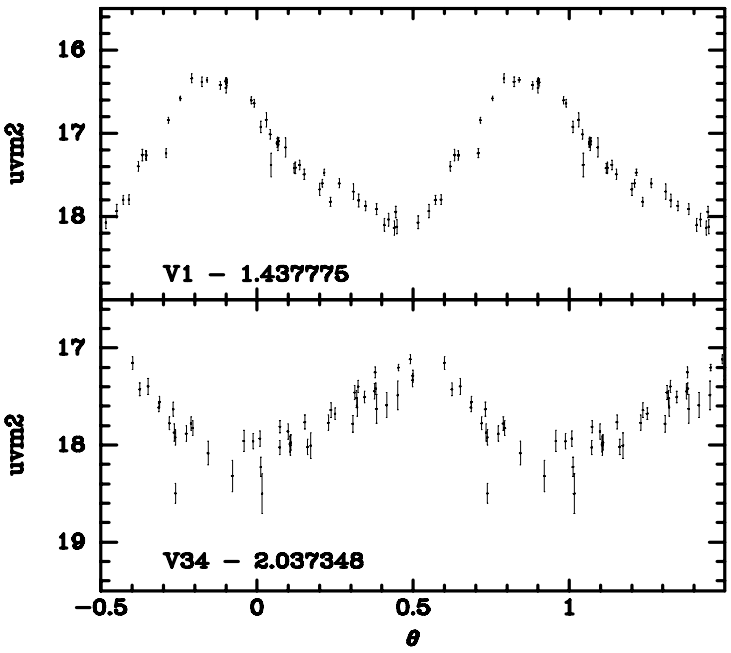

Fig. 17.— $uvm2$ light curves for two anomalous Cepheids in the globular cluster M 15.

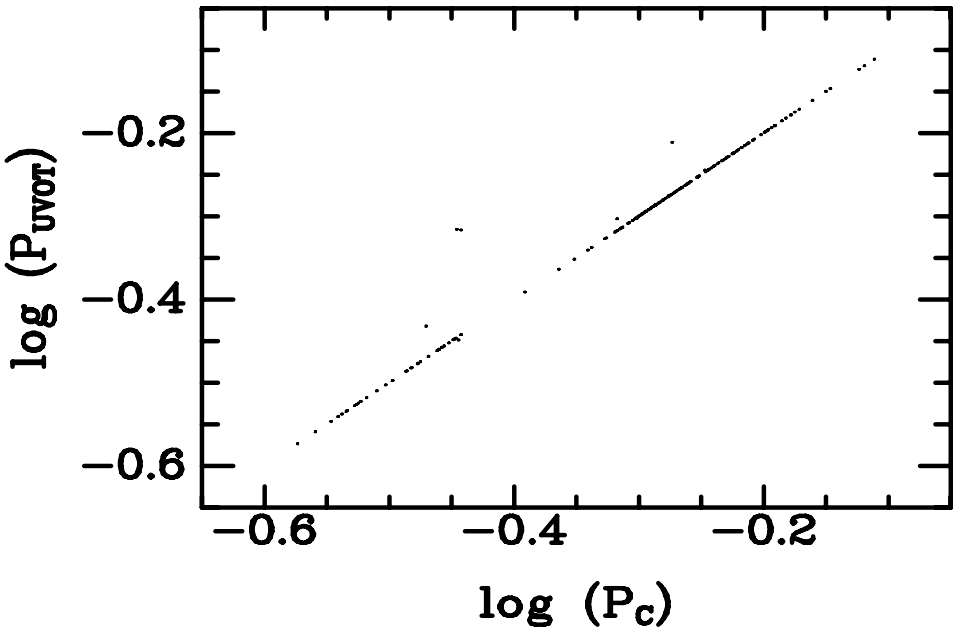

Fig. 18.— A comparison of the periods derived in this study (ordinate) against the compilation of C01 (abscissa) for the globular cluster M 3. The outliers are discussed in the text.

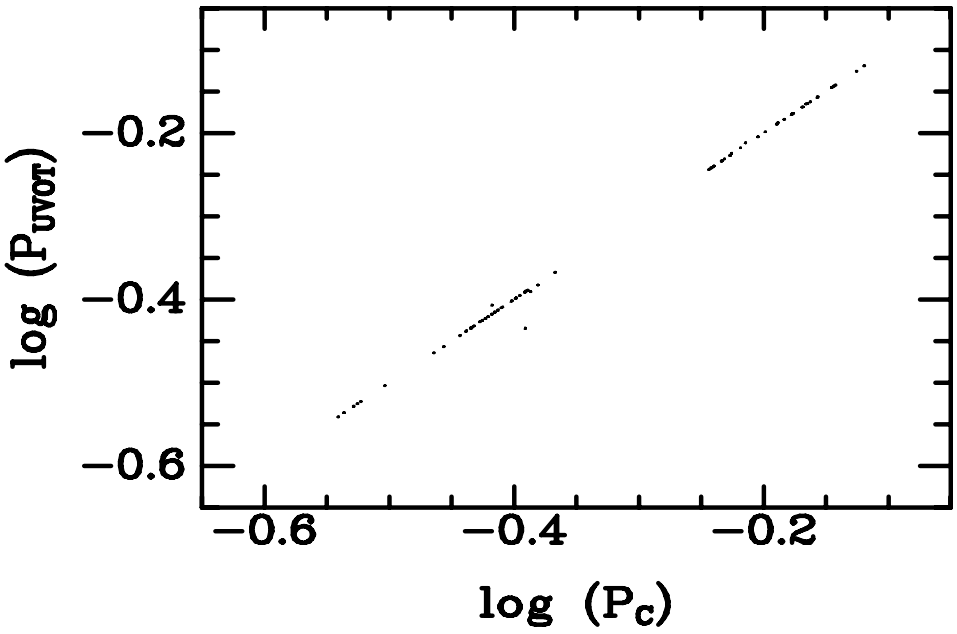

Fig. 19.— A comparison of the periods derived in this study (ordinate) against the compilation of C01 (abscissa) for the globular cluster M 15. The outliers are discussed in the text.

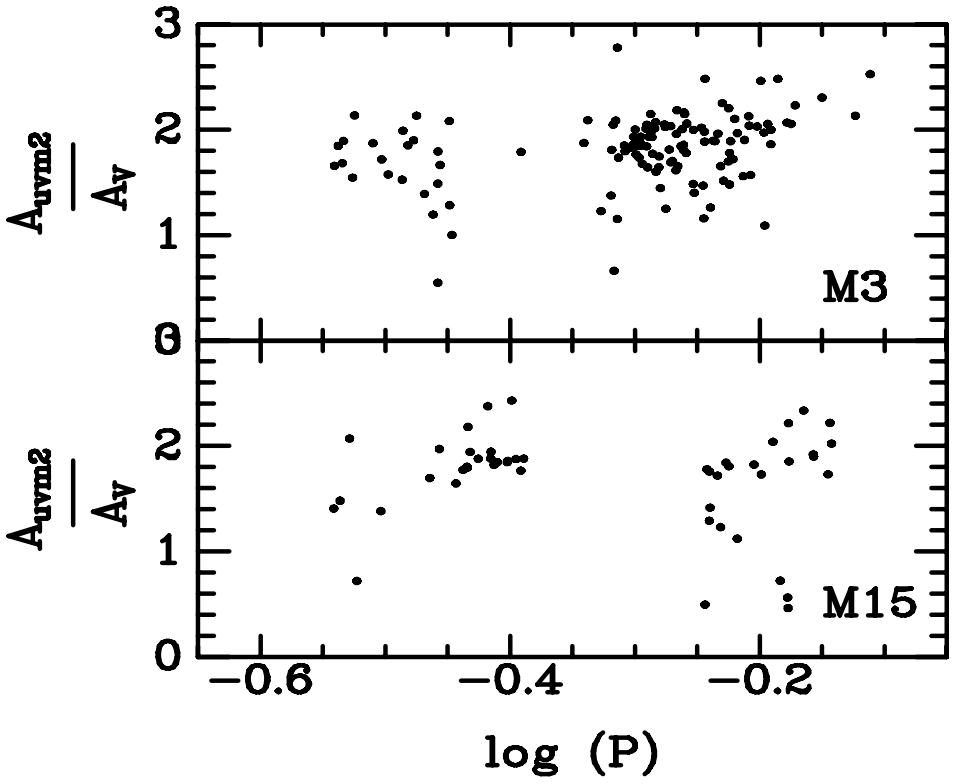

Fig. 20.— A comparison of the $uvm2$ pulsational amplitudes to the V amplitudes collected by C01. Note that the UV amplitudes are typically much larger than the optical amplitudes, indicating greater sensitivity to temperature changes.

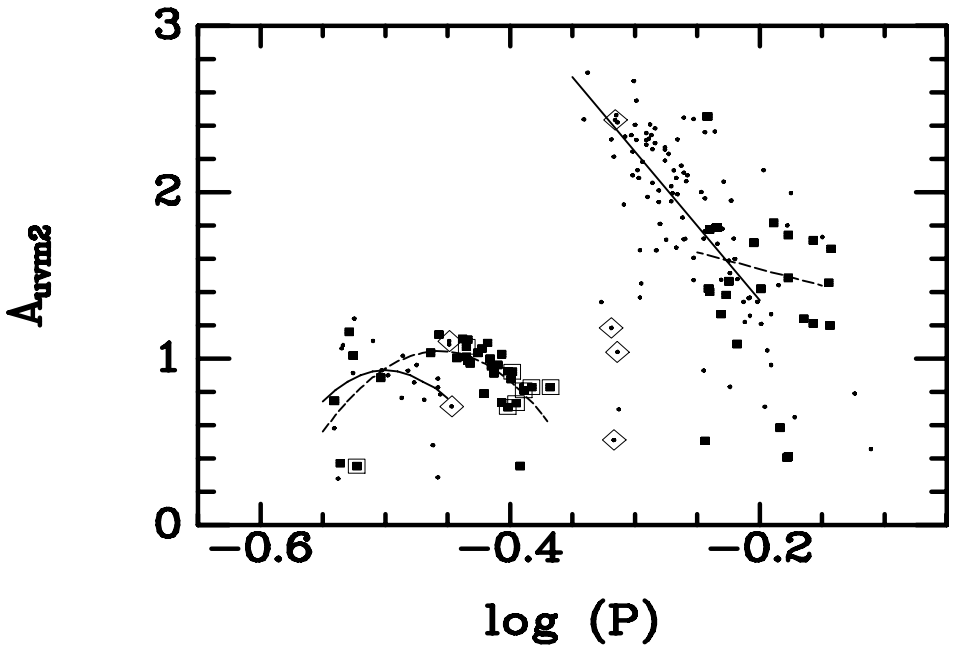

Fig. 21.— A Bailey diagram of period against pulsational amplitudes for the $uvm2$ data for M 3 (points) and M 15 (solid squares). Open diamonds and squares mark known double-mode pulsators in M 3 and M 15, respectively. The stars at longer periods ($log(P) > -0.4$) are the fundamental mode RRab pulsators while the stars at shorter periods ($log(P) < -0.4$) are the first overtone RRc pulsators. The lines denote fit period-amplitude relations for for M 3 (solid) and M 15 (dashed).

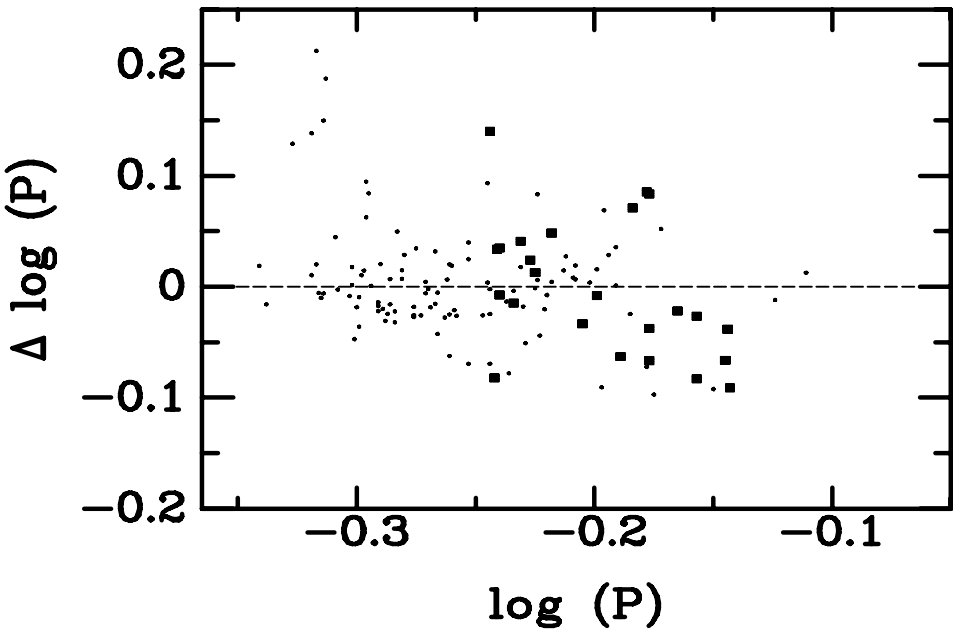

Fig. 22.— The period shift of RRab stars in M3 (points) and M15 (solid squares). The y-axis represent the displacement of the RRab pulsational period from the sequence of M 3.

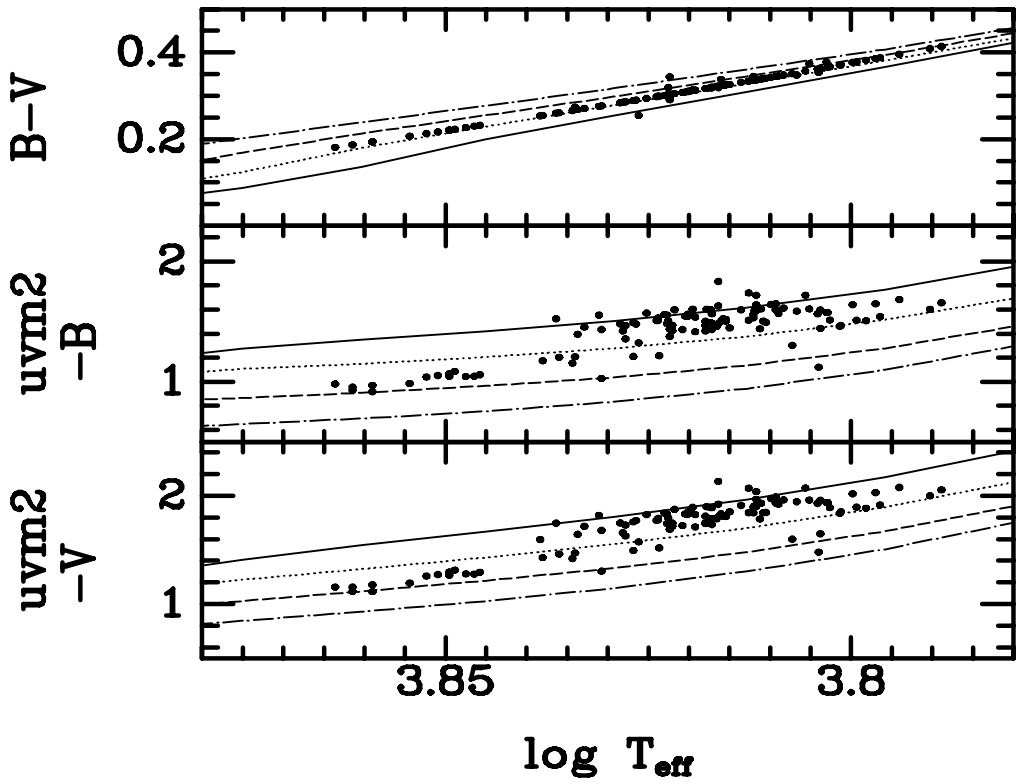

Fig. 23.— A comparison of $B-V$, $uvm2-B$ and $uvm2-V$ photometry to theoretical models of Castelli & Kurucz (2003). The lines show temperature-color relations for *log g* values of 2.0 (solid line), 2.5 (dotted), 3.0 (dashed) and 3.5 (dot-dash).

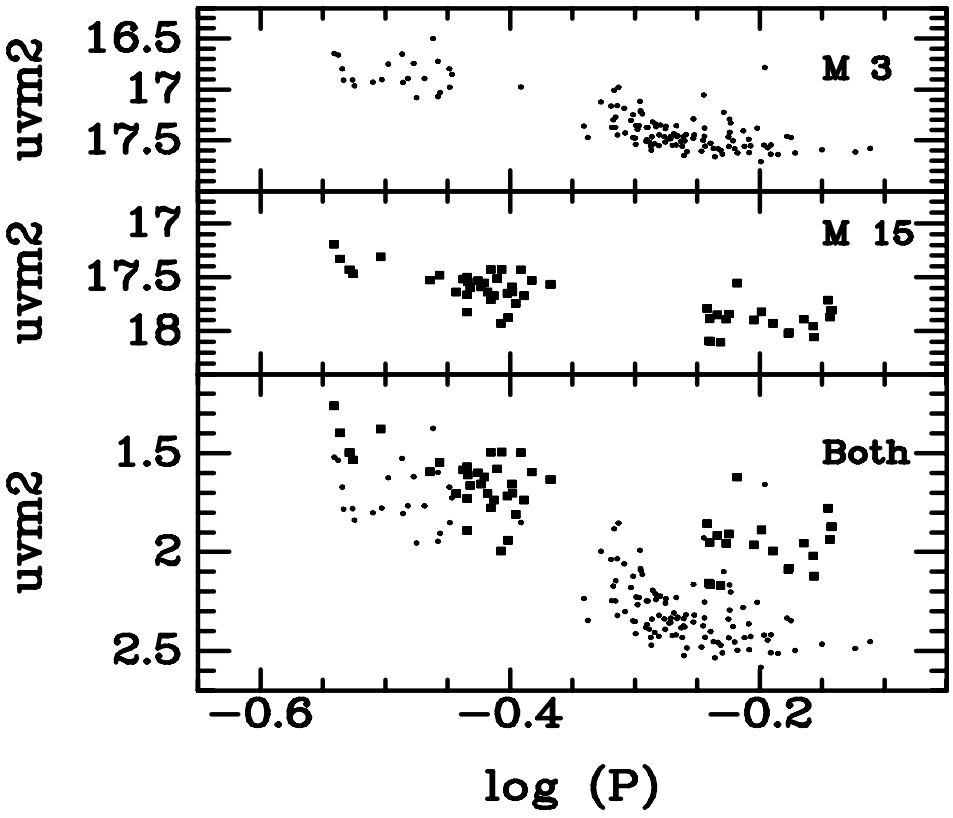

Fig. 24.— The period-luminosity relation of RR Lyrae stars in M3 (top) and M15 (middle). The outliers are likely blends. The bottom panel shows both clusters corrected for distance modulus and reddening.